



1 Strong influence of Black Carbon on aerosol optical properties in 2 Central Amazonia during the fire season

3 Rafael Stern¹, Joel F. de Brito², Samara Carbone³, Luciana Varanda Rizzo⁴, Jonathan Daniel Muller⁵ and
4 Paulo Artaxo⁴

5 ¹Climate and Environment Department, National Institute of Amazon Research, Manaus, 69060-001, Brazil

6 ²IMT Nord Europe, Institut Mines-Télécom, Université de Lille, Centre for Energy and Environment, 59000, Lille, France

7 ³Agrarian Sciences Institute, Federal University of Uberlandia, Uberlandia, Brazil

8 ⁴Physics Institute, University of São Paulo, 05508-090, Brazil

9 ⁵School for Climate Studies, Stellenbosch University, Stellenbosch, South Africa

10

11

12 *Correspondence to:* Rafael Stern (rafa.stern@yahoo.com.br)

13 **Abstract.** During the dry season, the Amazonian atmosphere is strongly impacted by fires, even in remote areas. However,
14 there are still knowledge gaps regarding how each aerosol type affects the aerosol radiative forcing. This work characterizes
15 the chemical composition of submicrometer aerosols and source apportionment of Organic Aerosols (OA) and Equivalent
16 Black Carbon (eBC) to study their influence on light scattering and absorption at a remote site in central Amazonia during the
17 dry season (August-December 2013). We applied Positive Matrix Factorization (PMF) and multi-linear regression models to
18 estimate chemical-dependent mass scattering (MSE) and extinction (MEE) efficiencies. Mean PM1 aerosol mass loading was
19 $6.3 \pm 3.3 \mu\text{g m}^{-3}$, with 77% of organics, grouped into 3 factors: Biomass Burning OA (BBOA), Isoprene derived Epoxydiol-
20 Secondary OA (IEPOX-SOA) and Oxygenated OA (OOA). The bulk scattering and absorption coefficients at 637 nm were
21 $17 \pm 10 \text{ Mm}^{-1}$ and $3 \pm 2 \text{ Mm}^{-1}$, yielding a single scattering albedo of 0.87 ± 0.03 . Although eBC represented only 6% of the PM1
22 mass loading, MSE was highest for the eBC ($13.58\text{-}7.62 \text{ m}^2 \text{ g}^{-1}$ at 450-700 nm), followed by BBOA ($7.96\text{-}3.10 \text{ m}^2 \text{ g}^{-1}$) and
23 ammonium sulfate (AS, $4.79\text{-}4.58 \text{ m}^2 \text{ g}^{-1}$). MEE was dominated by eBC (30.8%), followed by the OOA (19.9%) and AS
24 (17.6%). The dominance of eBC over light scattering, in addition to absorption, depicts a surprisingly high role of this
25 important climate agent, indicating the need to further investigate the chemical processing and interaction between natural and
26 anthropogenic aerosol sources over remote tropical forested areas.

27 1 Introduction

28 The Amazon is the largest hydrologic basin and contiguous tropical forest area of the planet, representing important carbon
29 reserves, sources of freshwater, and housing a large biodiversity (Andreae et al., 2015; Artaxo et al., 2013; Davidson et al.,
30 2012; Pöhlker et al., 2016). The strong coupling between climate and the biological functioning of the forest is a key factor in
31 the maintenance of the Amazonian ecosystem (Martin et al., 2010b; Pöhlker et al., 2012). The Amazonian atmosphere is



32 considered an important reactor, regulating its physical properties and chemical composition due to the high insolation and
33 humidity (Andreae, 2001). Despite the high temperatures, precipitation rates, and insolation during most of the year, an annual
34 cycle can be observed, with a wetter and less warm season and a drier and hotter season, whose length and period vary
35 depending on the region of the Amazon (Marengo et al., 2001).

36 During the wet season, the Amazonian atmosphere represents one of the few continental regions with episodic atmospheric
37 composition near pristine conditions (Andreae et al., 2015; Martin et al., 2010b; Pöhlker et al., 2018; Pöschl et al., 2010).
38 Particle number concentration during the cleanest period is a few hundred particles cm^{-3} , very similar to remote oceanic regions
39 (Andreae et al., 2015; Artaxo et al., 2013; Martin et al., 2010). However, during the dry season, forest fires are provoked in
40 order to clear forest areas for agriculture, and also as part of pasture and cropland management (Aragão et al., 2016; Berenguer
41 et al., 2021; Davidson et al., 2012). During these periods, forest fire emissions coupled with smaller rates of aerosol scavenging
42 lead to particle number concentration increases by a factor of 10 in remote forest areas (Artaxo et al., 2013; Pöhlker et al.,
43 2018). These stark seasonal differences in aerosol loading and composition have the potential to significantly modify the
44 coupling biosphere-atmosphere (Zaveri et al., 2022), which is expected to be exacerbated in the future due to extreme climatic
45 events in Amazonia (Flores et al., 2024).

46 Atmospheric aerosol particles influence climate through scattering and absorption of solar radiation (aerosol-radiation
47 interactions, ARI) and by affecting cloud formation and lifetime (aerosol-cloud interactions, ACI) (Forster et al., 2021).
48 However, the magnitude and the signal of global radiative forcing of aerosols still represent one of the largest uncertainties in
49 global climate models (Kuhn et al., 2010; Rizzo et al., 2013; Szopa et al., 2023). Uncertainties on the radiative forcing of
50 individual aerosol components are even higher (Myhre et al., 2013), with a direct impact on the accuracy of future climatic
51 scenarios (Forster et al., 2021). Carbonaceous aerosols (i.e. organic and black carbon) dominate the Amazonian atmosphere
52 (Artaxo et al., 2013). While Organic Aerosol (OA) originates from both primary emissions, as well as secondary formation
53 from gaseous precursors (Martin et al., 2010), black carbon is mostly primarily emitted from incomplete combustion, and in
54 remote areas of the Amazon it is associated with Amazonian or transatlantic forest fires (Artaxo et al., 2013; Holanda et al.,
55 2020). The sign and magnitude of the ARI forcing are dependent on several parameters such as particle origin, size distribution,
56 mixture and age, notably affecting the light-absorbing component of OA, termed brown carbon (Laskin et al., 2015; Saturno
57 et al., 2018b).

58 The secondary component of OA (SOA) in the Amazon has been shown to be a major component, notably during the wet
59 season (Chen et al., 2015; Shrivastava et al., 2019). Isoprene (2-methyl-1,3-butadiene, C_5H_8) is the most abundant VOC emitted
60 globally, mostly located in tropical forests such as the Amazon (Marais et al., 2016; Yáñez-Serrano et al., 2015). The formation
61 of isoprene-derived Secondary Organic Aerosol (SOA) is a sequence of complex reactions and depends on different factors,
62 such low concentrations of NO (a typical byproduct of fossil fuel combustion), and pre-existing aerosol particles where
63 isoprene can condense on (Brito et al., 2018; Caravan et al., 2024; Marais et al., 2016; Nah et al., 2019). One of the dominating
64 isoprene SOA pathways in the Amazon is through the OH attack, leading to hydroperoxy radicals and subsequently via the
65 HO_2 pathway (Shrivastava et al., 2019; Wennberg et al., 2018). This pathway can lead to different low-volatility products



66 generally termed IEPOX-SOA (Isoprene EPOXYdiols-Secondary Organic Aerosol) (Allan et al., 2014; Hu et al., 2015; Surratt
67 et al., 2010). Isoprene oxidation product mixing ratios were previously shown to be higher during the dry season above the
68 forest canopy, likely due to the higher insolation and temperature during this period, which favors the oxidative capacity of
69 the atmosphere and leaf emission potential (Yáñez-Serrano et al., 2015). IEPOX-SOA mass concentrations have been shown
70 to be significantly reduced during polluted conditions, associated with suppression due to urban NO emissions (de Sá et al.,
71 2017). Alternatively, a study in polluted urban plumes in West Africa found that SO₄ increase plays a larger role in enhancing
72 IEPOX-SOA loadings than NO in suppressing it (Brito et al., 2018). Secondary oxidized aerosol particles have been
73 demonstrated to be more efficient at scattering radiation than primary particles (Kleinman et al., 2020; Paredes-Miranda et al.,
74 2009; Reid et al., 2005; Smith et al., 2020).

75 Chemical composition, processes, and sources of atmospheric aerosol particles in the Amazon have been widely studied during
76 both the wet and dry seasons, in sites representing pristine conditions (Andreae et al., 2015; Chen et al., 2015; Martin et al.,
77 2010a) as well as strongly impacted by fires and urban pollution (Brito et al., 2014; Ponczek et al., 2021; de Sá et al., 2018;
78 Zaveri et al., 2022). Physical properties of radiation absorption and scattering were described (Artaxo et al., 2013; Nascimento
79 et al., 2021; Palácios et al., 2020; Rizzo et al., 2013; de Sá et al., 2019; Sena et al., 2013). However, the intrinsic optical
80 properties of each aerosol species are still rare (Velazquez-Garcia et al., 2023), notably associated with OA origins (Ponczek
81 et al., 2021). Our study details the chemical properties of submicrometer aerosol particles in a forest site in central Amazonia
82 during the dry season and their influence on radiation scattering and absorption. We applied positive matrix factorization
83 (PMF) to the organic fraction, associated mass extinction, absorption, and scattering efficiencies to different aerosol
84 components via multi-linear regression to improve our comprehension of their intrinsic properties, as well as estimate their
85 role on aerosol-radiation interaction in Central Amazonia during the dry season.

86 **2 Material and Methods**

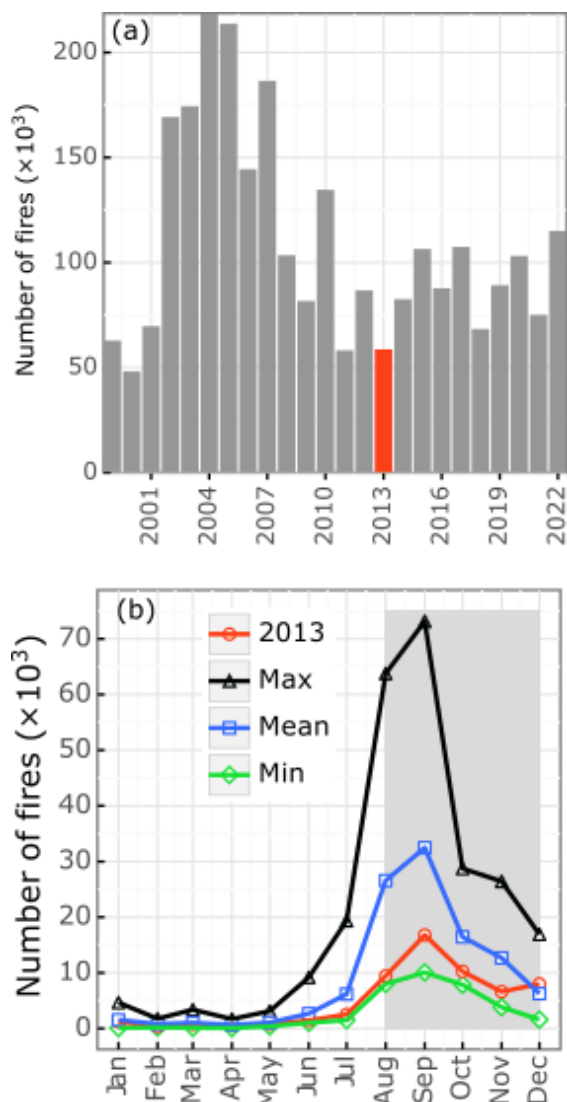
87 **2.1 Sampling site**

88 The measurements site is located 60 km northwest of the city of Manaus, Brazil, in the Cuieiras biological reserve
89 (2°35'39.24''S, 60°12'33.42''W), and referred to in this study as T0z (Martin et al., 2015; Whitehead et al., 2016). The
90 vegetation is characterized as *terra firme* (upland forest, not impacted by seasonally flooded), and the canopy is between 30 m
91 and 35 m high (Martin et al., 2010). As a result of steady northeasterly-easterly winds (Andreae et al., 2015; Araújo et al.,
92 2002), only rarely the site is impacted by Manaus emissions (Chen et al., 2015). The seasonality at the region of this site in
93 central Amazonia has been previously defined as the wet season from 1 December – 14 June, and the dry season from 15 June
94 – 30 November (Andreae et al., 2015). During the wet season, air masses reaching the site pass over more than 1,500 km of
95 undisturbed forest (Andreae et al., 2015; Pöschl et al., 2010). However, during the dry season, regional biomass burning
96 pollution can be detected at the site (Artaxo et al., 2013; Rizzo et al., 2013), as well as aerosol plumes advected from African
97 wildfires (Holanda et al., 2023). Our observations comprise from 1 August until 10 December 2013, sampling the atmosphere



98 at 38.8 meters above ground level. The instrumentation was located inside an air-conditioned container at the base of the tower.
99 A cyclone (50 % cut-off at 10 μm) was used at the entrance of the inlet. An automatic diffusion dryer (Tuch et al., 2009) kept
100 the relative humidity of the sampled air between 20% and 50%. Lodging for scientists/staff and a diesel generator were located
101 330m and 720m downwind (west) from the tower, respectively. The measurement tower has been shown to be practically
102 unaffected by the generator (Whitehead et al., 2016). The year of this study (2013) was characterized by a historical minimum
103 of fire detection over the last 20 years (Figure 1, (F. G. Assis et al., 2019)), providing an interesting outlook to assess the best
104 scenarios for a dry season in recent times, and thus evaluate atmospheric composition within targets and goals for the Amazon
105 forest preservation. The observation period here has been considered to fit entirely within dry-season atmospheric conditions.
106 The previous transitional (wet-dry) period occurred in June-July (Whitehead et al., 2016), and the subsequent (dry-wet) soon
107 after the end of our measurements.

108



109

110

111 **Figure 1: a) Number of fires in the Brazilian Amazon forest from 1999 to 2022, showing how 2013 (marked in red) is the lowest in**
112 **the past 20 years in terms of total number of fires, and b) mean (blue), maximum (black), minimum (green), and for 2013 (red)**
113 **monthly fires between 1999-2022 in the Amazon Basin. The gray area in b) marks the period of measurements in our study (01/Aug**
114 **– 10/Dec) (Instituto Nacional de Pesquisas Espaciais, 2024).**

115 2.2 Instrumentation

116 Non-refractory submicrometer aerosol composition was measured using a quadrupole Aerosol Chemical Speciation Monitor
117 (ACSM, Aerodyne Research Inc) (Ng et al., 2011), which is a compact version of the Aerosol Mass Spectrometer (AMS).
118 Instrument calibration consisted of injecting monodispersed (300 nm) aerosol particles of ammonium nitrate (AN) and



119 ammonium sulfate (AS). Aerosol particles were generated using an atomizer and subsequently dried, and size selected using
120 a Differential Mobility Analyzer. A collection efficiency of 0.5 has been adopted (Middlebrook et al., 2012), yielding a very
121 good agreement in particle mass considering measurements from different collocated instruments (S1). This method was
122 successfully used in previous studies (Brito et al., 2014; Sun et al., 2010), and the value of 0.5 agrees with other studies in the
123 Amazon during the dry season (de Sá et al., 2019) and during the transition from wet to dry season (Ponczek et al., 2021). The
124 measured ammonium (NH_4) mass concentrations were close to, or often lower than the detection limit of $0.28 \mu\text{m}^{-3}$ (Pöhlker
125 et al., 2018; Whitehead et al., 2016), and were therefore calculated based on nitrate (NO_3) and sulfate (SO_4) molar masses and
126 their mass concentrations, assuming neutralization as in Equation 1:

$$128 \quad \text{NH}_{4, \text{ predicted}} = 18 \times \left(\frac{\text{SO}_4}{96} \times 2 + \frac{\text{NO}_3}{62} \right) \quad (1)$$

129

130 Furthermore, the SO_4 and NO_3 ions were used to estimate AS and AN for the chemical-dependent optical properties analyses
131 (Section 3.3), assumed here to be their most abundant form given the very low NH_4 levels:

132

$$133 \quad \text{AS} = 132 \times \frac{\text{SO}_4}{96} \quad (2)$$

134

$$135 \quad \text{AN} = 80 \times \frac{\text{NO}_3}{62} \quad (3)$$

136

137 Size-resolved particle number size distribution from 10 to 450 nm was measured with a Scanning Mobility Particle Sizer
138 (SMPS, model 3081, TSI Inc.) coupled to a Condensation Particle Counter (CPC, model 3772, TSI Inc.) to provide equivalent
139 mobility particle diameter for singly charged particles (D_{pg} , (Wiedensohler et al., 2012). Aerosol light scattering coefficient
140 (σ_s) at 450 nm, 550 nm, and 700 nm (Anderson and Ogren, 1998) was measured using a Nephelometer (model 3563, TSI Inc.).
141 Calibration was performed using CO_2 as the high-span gas and filtered air as the low-span gas. The averaging time applied
142 was 60 minutes, and therefore the detection limits, defined as a signal-to-noise ratio of 2, for scattering coefficients are 0.08,
143 0.03, and 0.05 Mm^{-1} for 450, 550, and 700 nm, respectively (Anderson and Ogren, 1998). Since a PM10 inlet was used, the
144 “no-cut” factors were used for the truncation corrections (Anderson and Ogren, 1998). Scattering coefficients at 637 nm were
145 calculated from interpolation, assuming a power-law spectral dependency. A Multi Angle Absorption Photometer (MAAP,
146 model 5012, Thermo Electron Group, Waltham, USA) (Müller et al., 2011) measured aerosol light absorption coefficient (σ_a)
147 at 637 nm and was used to estimate equivalent Black Carbon (eBC) concentration, assuming an absorption cross-section value
148 of $6.6 \text{ m}^2 \text{ g}^{-1}$. Considering the conditions of the experiment, the MAAP detection limit for σ_a was of 0.13 Mm^{-1} (Petzold et al.,
149 2005).

150 Episodes of possible contamination from the city of Manaus and from the diesel generator were removed by filtering the
151 datapoints when either the wind direction was between $270\text{-}340^\circ$ (from our local wind direction measurements) or when the



152 calculated backtrajectories from the Hysplit model (Draxler and Hess, 1998) passed over Manaus coordinates, as in (Whitehead
153 et al., 2016) (Supplement S2).

154 **2.3 Optical properties**

155 Single Scattering Albedo (SSA, Equation 4) is a measure of the ratio of σ_s to the total radiation extinction coefficient ($\sigma_e = \sigma_s$
156 $+ \sigma_a$) by aerosol particles (Rizzo et al., 2013). Since the MAAP instrument only measures the σ_a at 637 nm wavelength, the σ_e
157 was calculated only for this wavelength using σ_s at 637 nm from the nephelometer, estimated using the scattering Angstrom
158 exponent (α_s , Equation 5).

$$159 \text{ SSA} = \frac{\sigma_s}{\sigma_s + \sigma_a} \quad (4)$$

160 The α_s is a measure of the dependence of radiation scattering on the light wavelength (λ), and it is an indication of particle size
161 (Rizzo et al., 2013; Saturno et al., 2018b; Schuster et al., 2006):

162

$$163 \ln \sigma_s = -\alpha_s \ln \lambda + \ln(\text{constant}) \quad (5)$$

164

165 After rain events and other moments when the atmosphere is very clean, both α_s for σ_e values are very low, and therefore the
166 ratio between them (SSA, Equation 4) becomes unrealistically high. We therefore calculated SSA for α_s for $\sigma_e > 1 \text{ Mm}^{-1}$.

167

168 **2.4 Statistical Analyses**

169 **2.4.1 Positive Matrix Factorization (PMF)**

170 The PMF (Positive Matrix Factorization) was used on the submicrometer non-refractory organic mass spectra in order to group
171 m/z ratios with similar temporal variability, supporting the identification of sources and processes that formed and transformed
172 atmospheric particles. A detailed description of the PMF can be found in (Paatero & Tapper, 1994; Ulbrich et al., 2009), and
173 it is an established methodology for aerosol source apportionment (Zhang et al., 2011). The model can be represented by the
174 following Equation. (6):

175

$$176 \mathbf{X}_{(m \times n)} = \sum \mathbf{G}_{(m \times p)} \cdot \mathbf{F}_{(p \times n)} + \mathbf{E} \quad (6)$$

177

178 Where \mathbf{X} is the input matrix of n (elements – m/z ratios) lines and m (number of samples) columns (Ulbrich et al., 2009). In
179 this study, the \mathbf{X} matrix had 2901 lines (1-hour averages for more than 4 months of measurements) and 70 columns (m/z
180 ratios). The receptor model aims to determine the number of p factors, representing sources or processes, their chemical
181 composition, and the relative contribution of each factor. \mathbf{G} is a matrix in which columns are the time series of the factors. \mathbf{F}
182 is a matrix in which lines are the profiles of the factors (mass spectra). \mathbf{E} represents the residuals, the part of the data that was



183 not modeled by any factor p . We used an IGORTM-based interface to apply the PMF analysis (Ulbrich et al., 2009). The PMF
184 ions were normalized to the organics concentration.

185 2.4.2 Multilinear Regression (MLR)

186 We used a Multilinear Regression (MLR) model to estimate the contribution of each aerosol chemical component to scattering,
187 absorption, and extinction coefficients, deriving the corresponding efficiencies (MSE, MAE, and MEE, respectively). The
188 scattering (σ_s) and absorption (σ_a) coefficients (Mm^{-1}) measured with the nephelometer and the MAAP (respectively) were the
189 dependent variables (response) and the species/factors were the independent (predictor) variables.

190 A generalization of the mass efficiency (ME) calculation is presented in Equation 7:

$$191$$
$$192 ME = \sum_i a_i x_i + r \quad (7)$$

193

194 Where ME can be MSE, MAE or MEE; x is the chemical species mass concentration; a_i is the efficiency of each component,
195 and r are the residuals. We used NNLS (Non-Negative Least Squares) from Python package Scipy version 1.5.2 (Virtanen et
196 al., 2020). To constrain the model to produce results with physical meaning, the coefficients a_i were constrained to be positive,
197 as in (Velazquez-Garcia et al., 2023). Since eBC is assumed to be the only absorbing component measured in this study with
198 the MAAP, a MLR could not be applied, and the MAE was considered to be equivalent to the cross-section value ($6.6 \text{ m}^{-2} \text{ g}^{-1}$,
199 Section 2.2).

200 3 Results and Discussion

201 3.1 Aerosol chemical composition

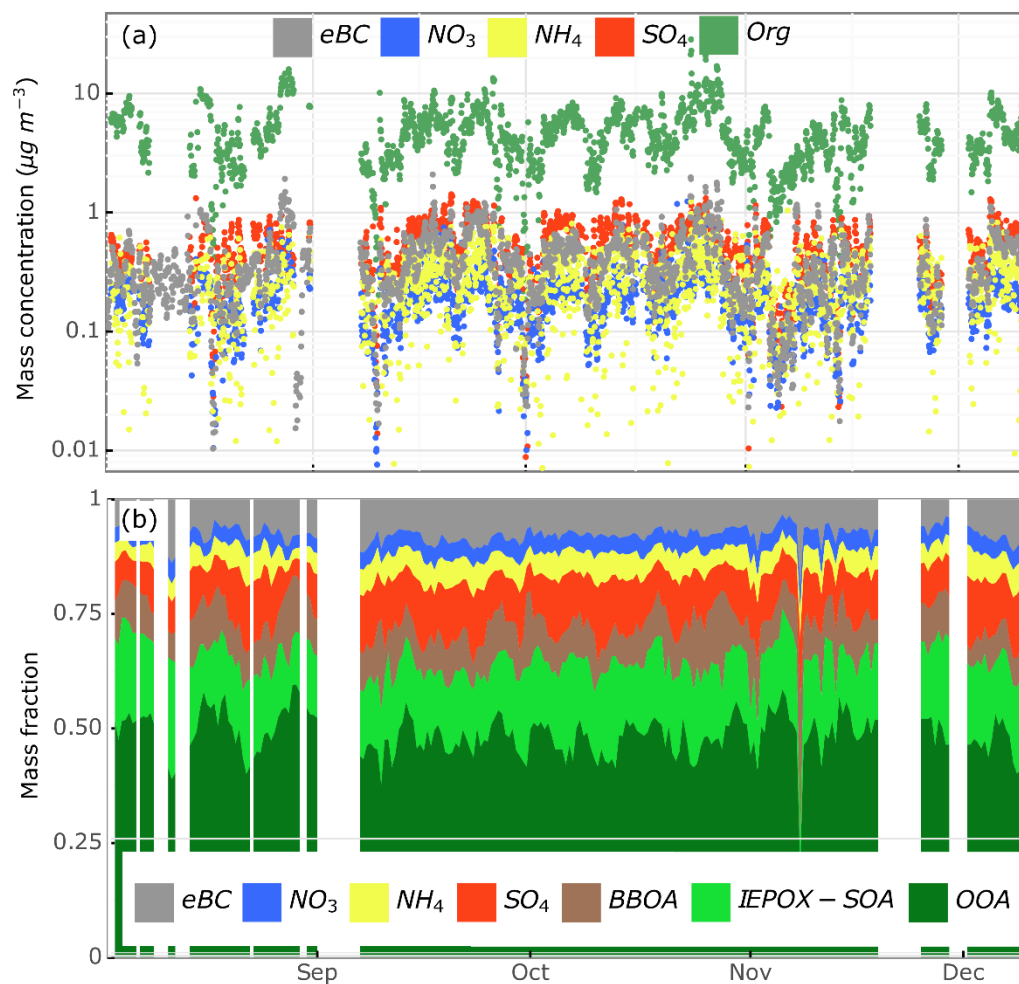
202 The total submicrometer ($\text{PM}_1 = \text{Organics} + \text{NO}_3 + \text{NH}_4 + \text{SO}_4 + \text{eBC}$) mean mass concentration during the observation period
203 was $6.3 \pm 3.3 \mu\text{g m}^{-3}$ (Table 1, Figure 1a). This represents about half of what was measured during the dry season of the following
204 year (2014, with much more fires, Figure 1) at a nearby site (ATTO tower, Amazon Tall Tower Observatory), with similar
205 conditions (Central Amazonia, isolated from major biomass burning focus or Manaus urban plume) ($10.5 \mu\text{g m}^{-3}$, (de Sá et al.,
206 2019)) and regions directly impacted by fires during the dry season ($12.4\text{-}13.7 \mu\text{g m}^{-3}$ (Brito et al., 2014; Ponczek et al., 2021)).
207 The PM_1 aerosol composition was dominated by the organic fraction, representing a mass fraction of $77 \pm 5\%$ (Table 1, Figure
208 2b). This is very similar to the wet season and wet to dry season transition in the same site ($> 80\%$ (Artaxo et al., 2013; Chen
209 et al., 2015; Whitehead et al., 2016)), but high compared to other continental urban areas, such as across Europe ($\sim 30\text{-}50\%$,
210 (Chen et al., 2022)) and lower than the strongly impacted by biomass burning region in Southwestern Amazonia (90% , (Brito
211 et al., 2014). Sulfate is the main soluble inorganic component of the aerosol mass fraction in the Amazon, both during the wet
212 and dry seasons (Fuzzi et al., 2007; Yamasoe et al., 2000). In our study, the mean SO_4 mass fraction was $9 \pm 3\%$ (Table 1,
213 Figure 2b), which is comparable to the ATTO site (Andreae et al., 2015). However, in Southwestern Amazonia, in areas



214 impacted by fresh biomass burning, the average SO₄ mass fraction was significantly lower (2-3% (Brito et al., 2014; Ponczek
215 et al., 2021)).

216 The eBC mass fraction was $6\pm 2\%$ (Table 1, Figure 2b), which is half than the fraction observed in the wet season at the same
217 site (11%), despite the much lower total submicrometer aerosol mass loading (Chen et al., 2015). Occasional urban pollution
218 from Manaus, long-range transport from Africa, and potential artifacts combined with much lower overall aerosol loading are
219 possible causes for this relatively higher eBC mass fraction in the wet season (Chen et al., 2015). In Southwestern Amazonia,
220 during the transition from dry to wet season, the contribution of eBC to PM₁ reached 15% (Ponczek et al., 2021). Nitrate had
221 a minor contribution during our observations ($3\pm 1\%$), with concentration levels comparable to the ATTO site (Pöhlker et al.,
222 2018), as well as Southwestern Amazonia (Brito et al., 2014; Ponczek et al., 2021)). The concentrations of organics and
223 inorganics follow similar patterns during the measurement period (Figure 2a). This can be an indication that the total mass
224 loading consists of well-mixed biomass burning and secondary aerosols, associated with large and regional-scale processes
225 (Darbyshire et al., 2019).

226



227

228 **Figure 2: Non-refractory submicrometer aerosol species and eBC mass (a) concentrations and (b) fractions at T0z. In (a) the vertical**
 229 **axis is the logarithm scale to facilitate the visualization of different species. In (a), data is shown in the original time stamp of 1 hour,**
 230 **while in (b) it was averaged to 12 hours in order to facilitate visualization.**

231

232 The PMF analysis yielded 4 factors, although 2 statistical factors were closely related to the Oxygenated Organic Aerosol
 233 (OOA) fraction, and the mass spectra, diurnal profile, and time series of these factors did not present enough differences to
 234 justify their separation (Supplements S3 and S4). Therefore, these 2 factors were manually summed in order to generate a 3
 235 factors solution, which was different from the factors found in the 3 factors solution presented by the PMF. In (Ulbrich et al.,
 236 2009), the authors describe how one PMF resulting statistical factor can split into various other factors which, after added,
 237 represent the real factor. The recombination often considers similarities between the statistical factors in the mass spectra,
 238 diurnal profile and time series (Carbone et al., 2013). In our study, the identification of the factors was further confirmed with
 239 the correlation between the PMF statistical factors and the inorganic aerosols, with the eBC (Supplement S4) and diurnal



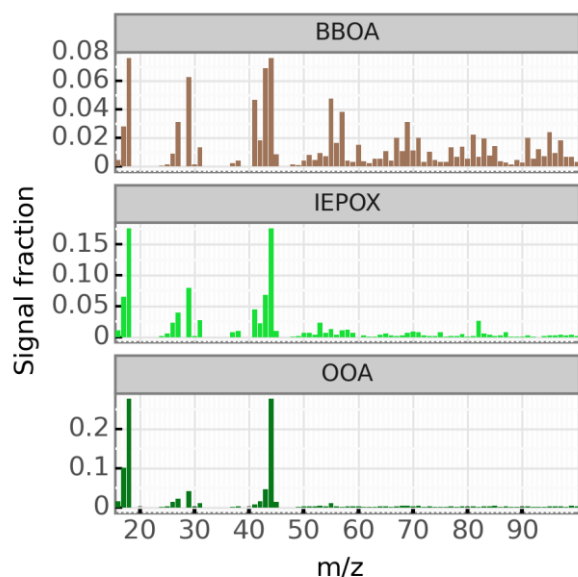
240 profile analyses. The 3 factors were identified as BBOA (Biomass Burning Organic Aerosol), OOA (Oxygenated Organic
241 Aerosol) and IEPOX-SOA (Isoprene derived Epoxydiol–Secondary Organic Aerosol), and they represent together 99% of the
242 measured submicrometer organic aerosol mass, with 1% of residuals. The correlation between BBOA and NO₃ and SO₄ is
243 comparable with findings in Southwestern Amazonia (Brito et al., 2014).

244 **Table 1 - Dry season (01/Aug – 10/Dec) mean mass concentration ($\mu\text{ m}^{-3}$), standard deviations, and percentile range**
245 **(10-90, in parenthesis) of the species measured by the ACSM and MAAP (eBC).**

	Mass concentration ($\mu\text{g m}^{-3}$)	Mass fraction
Total PM1	6.3±3.3 (2.7-10.3)	100%
Organics	4.9±2.7 (2.1-7.9)	77±5%
<i>BBOA</i>	0.6±0.6 (0.2-1.1)	9±5%
<i>IEPOX-SOA</i>	1.0±0.5 (0.4-1.7)	17±5%
<i>OOA</i>	3.2±1.5 (1.3-5.5)	51±6%
NO ₃	0.2±0.1 (0.1-0.3)	3±1%
NH ₄	0.3±0.1 (0.0-0.5)	4±1%
SO ₄	0.5±0.3 (0.2-0.9)	9±3%
eBC	0.4±0.3 (0.1-0.7)	6±2%

246
247 The largest contribution PMF-derived statistical factor in our study was OOA, which contributed to 51±6% of the PM1 (Table
248 1), and 65% of the organic mass. It presented the largest m/z 44 fraction (Figure 3), and therefore, this is the factor with the
249 highest estimated O:C ratio (Chen et al., 2015). The high oxidation level indicates highly aged particles and may lose some of
250 their original chemical signatures, in terms of elementary ratios, during the aging process (Jimenez et al., 2009). The m/z 44
251 is formed mainly by the fragment CO₂⁺, typical of the thermal decarboxylation of the organic acids groups (Alfarra et al.,
252 2004). The more aged the aerosols, the more chemically similar they become, which makes the task of separating them into
253 different factors with distinctive characteristics very difficult. Therefore, the OOA factor probably groups aerosol particles
254 from different sources, and their common characteristic is that they are probably originating relatively distant from the
255 sampling site. This factor is a major component of basin-wide haze observed during biomass burning season, associated with
256 the transport from eastern Amazonia into remote central regions at the center of the basin (Darbyshire et al., 2019).

257



258

259 **Figure 3: PMF Mass spectra composition of each statistical factor and its relative contribution to the total submicrometer organic**
260 **aerosol mass. It is possible to observe typical tracer ions such as m/z 60 and m/z 73 that characterize the BBOA factor, and also the**
261 **m/z 82 in the IEPOX-SOA factor.**

262

263 The production of IEPOX-SOA generally leads to the production of markers in the atmosphere, such as the 2-methyltetrol
264 and the 3-methylfuran (m/z 82, C₅H₆O⁺). These markers may not originally exist in the IEPOX-SOA molecule due to their
265 extremely high volatility, but they can be formed during the decomposition of some IEPOX-SOA species, such as 3-
266 methyltetrahydrofuran-3,4-diols (3-MeTHF-3,4-diols) (Lin et al., 2012). The organic fraction in the m/z 82 is therefore
267 important for the identification of the IEPOX-SOA factor, despite its low contribution to the submicrometer organic aerosol
268 mass fraction (usually below 4%). Beyond that, most of the other m/z are common to other factors, making the m/z 82
269 distinctive of the IEPOX-SOA, which can also be identified by the m/z 53 (C₄H₅⁺) and m/z 75 (C₃H₇O₂⁺) (Allan et al., 2014;
270 Lin et al., 2012; Xu et al., 2015a). The lifetime of IEPOX-SOA in the boundary layer is estimated to be about 2 weeks (Hu et
271 al., 2016). The IEPOX-SOA mean mass concentration in our study was 1.0±0.5 µg m⁻³ (Table 1, Figure 4). Previous studies
272 reported 0.26 µg m⁻³ during the wet season (Chen et al., 2015), while downwind of Manaus it was around 0.5 µg m⁻³ during
273 background conditions, and 0.1 µg m⁻³ during polluted conditions (de Sá et al., 2017). It is important to note that at T0z, while
274 the organic particle loading typically increases by an order of magnitude from the wet to the dry season (Artaxo et al., 2013),
275 we estimated that IEPOX-SOA increases about a factor ~3. The relative contribution of IEPOX-SOA to organics during the
276 wet season was estimated to be 34%, in contrast to the 17% found in this study (Table 1), which is likely the result of a complex
277 balance between increased isoprene emissions (Yáñez-Serrano et al., 2015), sulfate abundance and increased pollution levels
278 (including NO_x from forest fires, and biomass-burning related aerosol particles). The relative contribution of IEPOX-SOA to
279 the total PM1 mass was relatively constant during the whole measurement period (Figure 2b), as well as most of the other



280 species (with the exception of some episodes). This indicates that an atmospheric dynamics of rain/dilution controlling the
281 chemical composition could be more important than the influence of local sources of particles, confirming the regional haze
282 hypothesis raised by (Darbyshire et al., 2019).

283 The correlation (Pearson coefficient = 0.7) observed between the IEPOX-SOA factor and AS (Supplement S4.1) is similar to
284 the correlation measured in regions affected by urban pollution in the Amazon, Africa and USA ($R^2 = 0.37-0.48$ (Brito et al.,
285 2018; Budisulistiorini et al., 2013; de Sá et al., 2017)). Sulfate is the main aqueous phase particle in which isoprene products
286 use to condense on (Budisulistiorini et al., 2013; Kroll et al., 2006; Lin et al., 2012; Marais et al., 2016; Surratt et al., 2010;
287 Xu et al., 2015b), and therefore a positive and moderate-high correlation is expected. eBC presents a similar correlation with
288 IEPOX-SOA as AS (Supplement S4), but the correlation is even higher with the other PMF statistical factors, especially OOA
289 (Pearson coefficient = 0.85, Supplement S4). Since OOA corresponds to more than half of PM1 (Table 1), this high correlation
290 indicates that most of the submicrometer aerosols measured during the dry season in Central Amazonia are, in general,
291 influenced by biomass burning emissions, since eBC is an important combustion tracer. However, the fact that the eBC
292 correlation is higher with the OOA factor than with BBOA (which constitutes only 9% of PM1, Table 1, Supplement S4)
293 indicates that long-range transport of aged and internally well mixed biomass burning plumes plays a more important role than
294 nearby fire sources (Darbyshire et al., 2019).

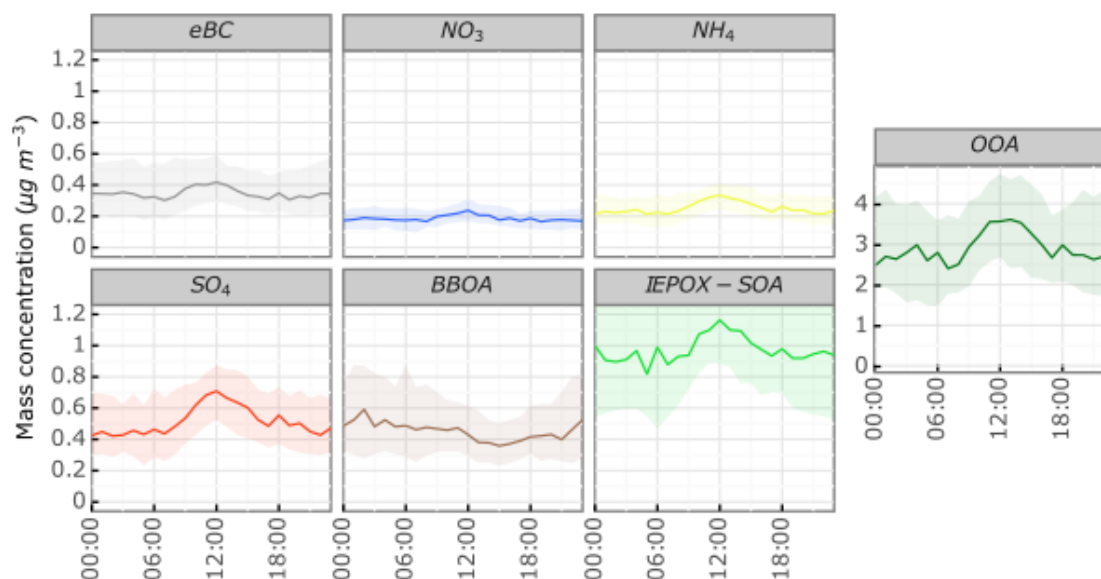
295 The BBOA factor can be identified by the presence of the m/z 60 and m/z 73 (Figure 3), which are dominated by the $C_2H_4O_2^+$
296 and the $C_3H_5O_2^+$ fragments. These fragments are originated from levoglucosan and other similar anhydro-sugars (such as
297 manosan and galactosan). Levoglucosan (1,6- α -D-anhydroglucopyranose, $C_6H_{10}O_5$) is known as a biomarker of biomass
298 burning emissions due to its production from the pyrolysis of carbohydrates as cellulose (Alfarra et al., 2007; Artaxo et al.,
299 2013; Chen et al., 2009; Lee et al., 2010). The signal fraction of m/z 60 for the BBOA factor in our study was 1.5%, which is
300 5 times higher than the 0.3% threshold typically used as an appropriate background fraction for biomass burning (Cubison et
301 al., 2011). OOA presented a m/z 60 signal fraction of 0.2%, while IEPOX-SOA presented a negligible signal.

302 The BBOA diurnal profile is different from that of the other PMF factors (Figure 4). While the OOA and IEPOX-SOA mass
303 concentrations increase during the daytime due to photochemical oxidation processes, the BBOA mass concentration is fairly
304 constant (Figure 4). Since the BBOA is a biomass-burning indicator, it is composed of mostly primary particles, so its
305 concentration does not depend on photochemical activity. This pattern is different than the stark decrease in mass
306 concentrations of fresh biomass burning particles during daytime, observed in southwestern Amazonia (Brito et al., 2014),
307 where there were constant local sources of fires and the diurnal cycle was mostly determined by the boundary layer increasing
308 and diluting the particles in a bigger area during daytime (Andreae et al., 2015). The lack of a clear diurnal pattern in our study
309 for BBOA seems to confirm the regional origin of the aerosol particles, likely transported from distant biomass burning sources
310 in the eastern parts of the basin, and long-range transport with complex interactions between residual and nocturnal layers
311 (Darbyshire et al., 2019). An additional confirmation of the long-range transport is the relatively flat pattern of the eBC diel
312 cycle, although there is a small but noticeable increase in the eBC diurnal mass concentration during daytime (Figure 4), which
313 may indicate some lensing effect due to the increase in the particle coating (Denjean et al., 2020). While the diel cycle of the



314 NH_4 and NO_3 show practically no variation, the SO_4 indicates the influence of photochemical processes (Figure 4) or
 315 atmospheric transport. The higher boundary layer in the afternoon (Fisch et al., 2004) may favor the downward transport of
 316 long-distance particles (Darbyshire et al., 2019). An additional possible explanation for this observed increase in SO_4 during
 317 the afternoon is biogenic sources of SO_4 precursors.

318 As the OOA and the IEPOX-SOA factors represent together around 68% of the total mass fractions of the submicron particles
 319 during our study, and conversely, eBC and BBOA represent only 15%, the importance of the atmospheric photochemical
 320 activity in Central Amazonia becomes evident. Well-preserved parts of the Amazon are strongly affected by the regional
 321 transport of well-processed biomass burning plumes, overwhelming the local biogenic processes that usually modulate the
 322 diurnal behavior of secondary aerosol development (Artaxo et al., 2013; Darbyshire et al., 2019).



323
 324 **Figure 4: Diurnal profile (local time) of the PMF derived statistical factors, the inorganic chemical species and eBC mass**
 325 **concentrations for the whole period of measurements (1 August – 10 December, 2013). The lines represent mean values, and the**
 326 **shaded areas represent the standard deviations. The OOA factor, shown separately, has a different vertical scale.**

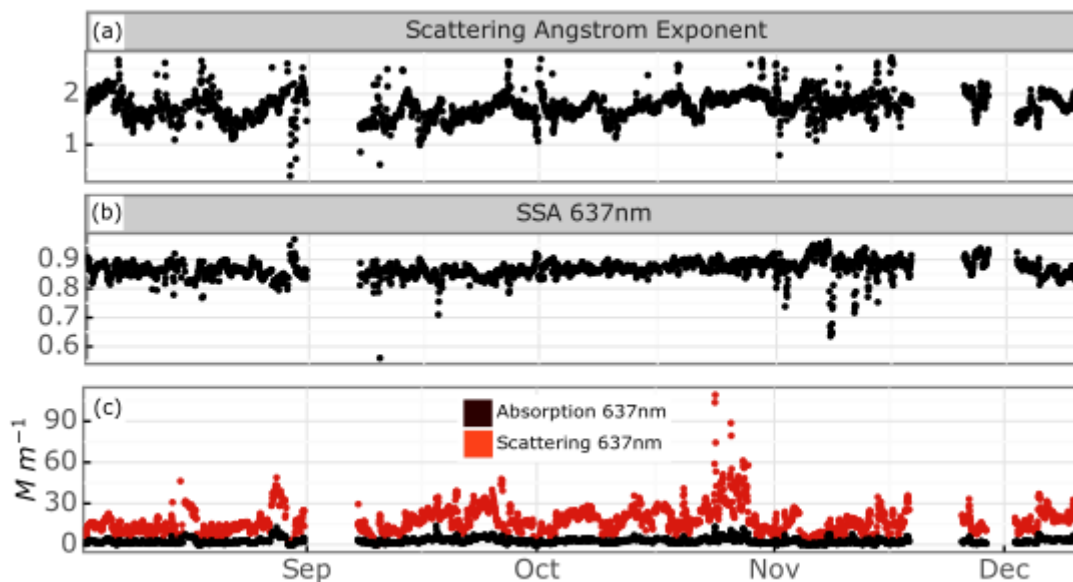
327 3.2 Physical properties

328 The mean scattering coefficient at 637 nm in our study was $17 \pm 10 \text{ Mm}^{-1}$ (Table 2), which is similar to the values reported for
 329 the same site and at the ATTO site during the dry season in previous years (Rizzo et al., 2013) and lower than observations
 330 close to biomass burning sources ($32\text{--}80 \text{ Mm}^{-1}$ (Artaxo et al., 2013; Ponczek et al., 2021)). In the dry season, fine mode particles
 331 predominate and are more efficient at scattering radiation than coarse mode dominated biogenic particles in the wet season
 332 (Rizzo et al., 2013). The absorption coefficient mean value was $3 \pm 2 \text{ Mm}^{-1}$ (Table 2, Figure 5, Section 2.2).

333



334



335

336 **Figure 5: Time series of: a) the Scattering Angstrom Exponent (unitless), b) Single Scattering Albedo (SSA) at 637 nm (unitless),**
337 **and c) absorption and scattering coefficients at 637 nm (Mm^{-1}).**

338

339 The mean SSA observed in our study (0.87 ± 0.03 , Table 2) was very similar to the SSA reported for the nearby ATTO site
340 (Saturno et al., 2018b). In previous years (2009-2012) at the same site as in our study, SSA varied from 0.84 to 0.91 from the
341 wet to the dry season respectively. The dominance of organics and the relatively high SO_4 fraction in our study (9%, Table 1)
342 are probably important factors for the high SSA (Artaxo et al., 2013; Rizzo et al., 2013). SSA was lower (0.77 ± 0.08 at 637
343 nm) during the transition from dry to wet season in a site highly impacted by fires in southwestern Amazonia (Ponczek et al.,
344 2021).

345 The mean value for the scattering Angstrom exponent in our study was 1.76 ± 0.26 (Table 2), which is very similar to the
346 1.70 ± 0.41 and the 1.71 ± 0.24 measured in the dry seasons of previous years at the same site and at the nearby ATTO station
347 (Rizzo et al., 2013; Saturno et al., 2018b), and the 1.65 ± 0.37 measured during the dry season at a site more impacted by forest
348 fires (Ponczek et al., 2021). However, it was higher than the 1.48 ± 1.12 (although within the high variability range) and the
349 1.29 ± 0.50 measured in wet seasons of previous years at the same station and the ATTO site (Rizzo et al., 2013; Saturno et al.,
350 2018b). Higher scattering Angstrom exponent values are usually related to a greater proportion of fine mode particles in the
351 aerosol population (Andreae et al., 2015), and in our case, it is probably related to the occurrence of fresh biomass burning
352 particles.

353

354 **Table 2 – Optical properties mean and standard deviation (in parentheses) for the whole study period for different**
355 **wavelengths.**



Optical property	Wavelength (nm)	Mean
Scattering coefficient (Mm^{-1})	450	32±19
Scattering coefficient (Mm^{-1})	550	22±13
Scattering coefficient (Mm^{-1})	637	17±10
Scattering coefficient (Mm^{-1})	700	14±8
Absorption coefficient (Mm^{-1})	637	3±2
Single Scattering Albedo (Mm^{-1})	637	0.87±0.03
Scattering Angstrom Exponent		1.76±0.26

356

357 3.3 Chemical-dependent optical properties

358 We applied the multiple linear regression (Section 2.4.2) to our dataset and the resulting coefficients successfully predicted
359 the observed scattering (Figure 6), confirming the validation of this methodology to estimate the specific contribution of each
360 chemical group to the optical properties. All the coefficients of the multilinear regression of all the wavelengths were
361 statistically significant ($p < 0.001$) for both MSE and MEE. The MSE of the PMF factors decreased as a function of wavelength
362 (Figure 7), in agreement with a previous study (Ponczek et al., 2021). Regarding the inorganic species, this decrease was also
363 observed in the AN, but absent in the AS, which showed no wavelength dependency (Figure 7). The highest MSE values were
364 attributed to eBC (Table 3, Figure 7a), followed by the BBOA. The MSE values of the eBC, BBOA and OOA components
365 calculated in our study at 637 nm were *circa* 180%, 67% and 43% respectively compared to (Ponczek et al., 2021). MSE of
366 AS in our study was between 4.58-4.79 $m^2 g^{-1}$ (considering wavelengths from 450-700 nm, Table 4), which is almost double
367 of the 2.5±0.6 $m^2 g^{-1}$ fine mode average of 93 observations of a variety of regions (urban, remote, rural continental,
368 ocean/marine) and seasons, and using different methods, mostly at 550 nm (Hand and Malm, 2007). Despite the small
369 variability, lower MSE was reported for drier and cleaner environments, and higher MSE was found in more polluted regions
370 and larger particle sizes (Hand and Malm, 2007), which may partially explain the higher values found in our study – in a wet
371 climate and during the forest fires season when the atmosphere can resemble that of highly polluted regions (Artaxo et al.,
372 2013). A recent study in an area highly impacted by urban pollution in France reported MSE for AS ranging from 4.8-7.1 m^2
373 g^{-1} (450-635 nm) (Velazquez-Garcia et al., 2023), resembling more similar results to our study for the lower wavelengths.
374 Concerning the contribution of AN to the PM1 mass concentration, we tested the MLR removing AN, and the results were
375 comparable, especially for eBC (Supplement Table S5.1). We also tested the robustness of the method by running 100 times
376 MLR on random 50% of the data, yielding similar results (Supplement Table S5.2).

377 Aerosol particles which typically absorb radiation are also known to have significant scattering efficiencies, highly dependent
378 on their sizes (Bond and Bergstrom, 2006). Biomass burning aerosols have been previously associated with high scattering
379 efficiencies (Hand and Malm, 2007; Malm et al., 2005). However, no clear particle size dependency was observed for the



380 radiation scattering in our study (Figure 6). Our result of a pronounced MSE of the eBC represents an opposite trend than the
381 observed in the transition from the dry to the wet season at a site more impacted by the fires, where the MSE of BBOA was
382 higher than eBC's (Ponczek et al., 2021).

383 When the mass concentration is considered, the relative contribution of eBC to the scattering in all the measured wavelengths
384 is about 20-25% of the total scattering (Figure 7b), comparable to Southwestern Amazonia (Ponczek et al., 2021), despite our
385 site having a significantly lower eBC concentration. The contribution of AS and AN to MSE was from 20% to 30% with
386 increasing wavelength (Figure 7b), less than half of that in urban sites in Europe (e.g. 67% in Northern France, (Velazquez-
387 Garcia et al., 2023), but about twice as high as during an extreme pollution haze episode in Beijing (Wang et al., 2015).

388 When considering the total light extinction (scattering + absorption), the relative contribution of eBC reaches about 30%
389 (Figure 8), which is comparable to the work in highly urbanized region in Europe (Velazquez-Garcia et al., 2023), however
390 significantly lower than the $76 \pm 20\%$ observed in urban pollution in China (Yu et al., 2010). By using the MSE and MEE ratios,
391 we calculated specific SSA for the eBC, obtaining a value of 0.57. This means that 57% of the light extinction provoked by
392 the eBC is scattered rather than absorbed, which is higher than the eBC specific SSA of 0.46 based on previous studies in more
393 polluted conditions (Ponczek et al., 2021; Velazquez-Garcia et al., 2023). SSA of eBC has been described as typically ranging
394 from 0.3 to 0.4, with higher values associated to heavy coating (Luo et al., 2020). Evidence of coating increasing elemental
395 carbon scattering efficiency has been found in the past (He et al., 2015; Yu et al., 2010), however other studies found that thick
396 coating in eBC lowered scattering coefficients (Darbyshire et al., 2019).

397 A previous study found that eBC absorption cross-section for the Amazon was $12.3 \text{ m}^2 \text{ g}^{-1}$ (Saturno et al., 2018b), and we
398 tested our dataset applying this value. The result is that eBC mass concentrations would become half of what they are reported,
399 with no change in σ_a , SSA, but MSE would double, while eBC contribution to MEE (Figure 8) would remain unchanged. Due
400 to some methodology differences between our study and (Saturno et al., 2018a) (they measured refractory Black Carbon using
401 a single-particle soot photometer SP2, with a higher cut-off, possibly leading to a sub-estimation of the mass), and the fact that
402 applying the absorption cross-section value they found would make MSE of eBC be an order of magnitude higher than the
403 others (Supplement Figure S6), we opted to remain with the more established value of $6.6 \text{ m}^2 \text{ g}^{-1}$.

404 The OOA factor presented a relatively high relative contribution to MSE and MEE (Figures 8b and 9) due to its high mass
405 relative contribution to the total PM1 mass (Table 1), although its MSE is relatively low (Figure 7a). Our results show an
406 increase in AS relative fraction of contribution to MSE with increasing wavelength (from 10% to 20%, Figure 7b), while OOA
407 decreased (from 30% to 20%, Figure 7b). The relative contributions to MSE of the OOA and BBOA were about twice as high
408 in a site more directly impacted by fires during the dry season than in our study (Ponczek et al., 2021).

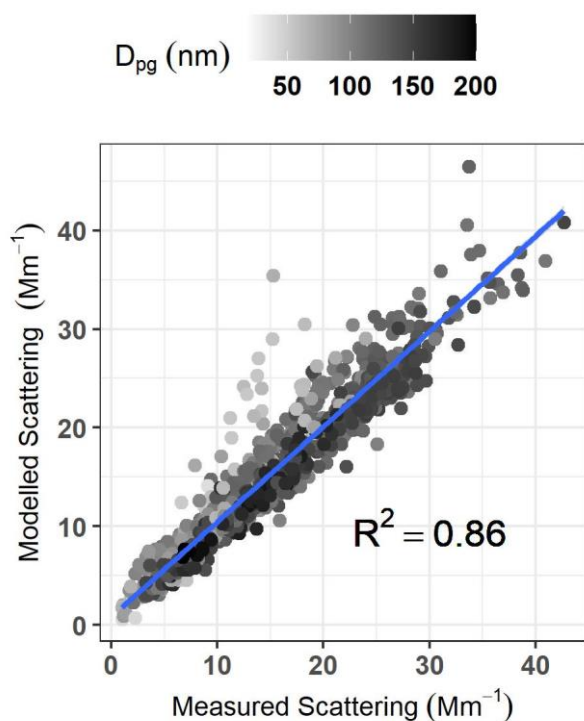
409 **Table 3 – MEE, MAE and MSE for different wavelengths and aerosol components with standard errors. All the**
410 **coefficients were statistically significant for all the wavelengths for MSE and MEE ($p < 0.001$).**

Wavelength (nm)	MSE ($\text{m}^2 \text{ g}^{-1}$)				MAE	MEE
	450	550	637	700	637	637



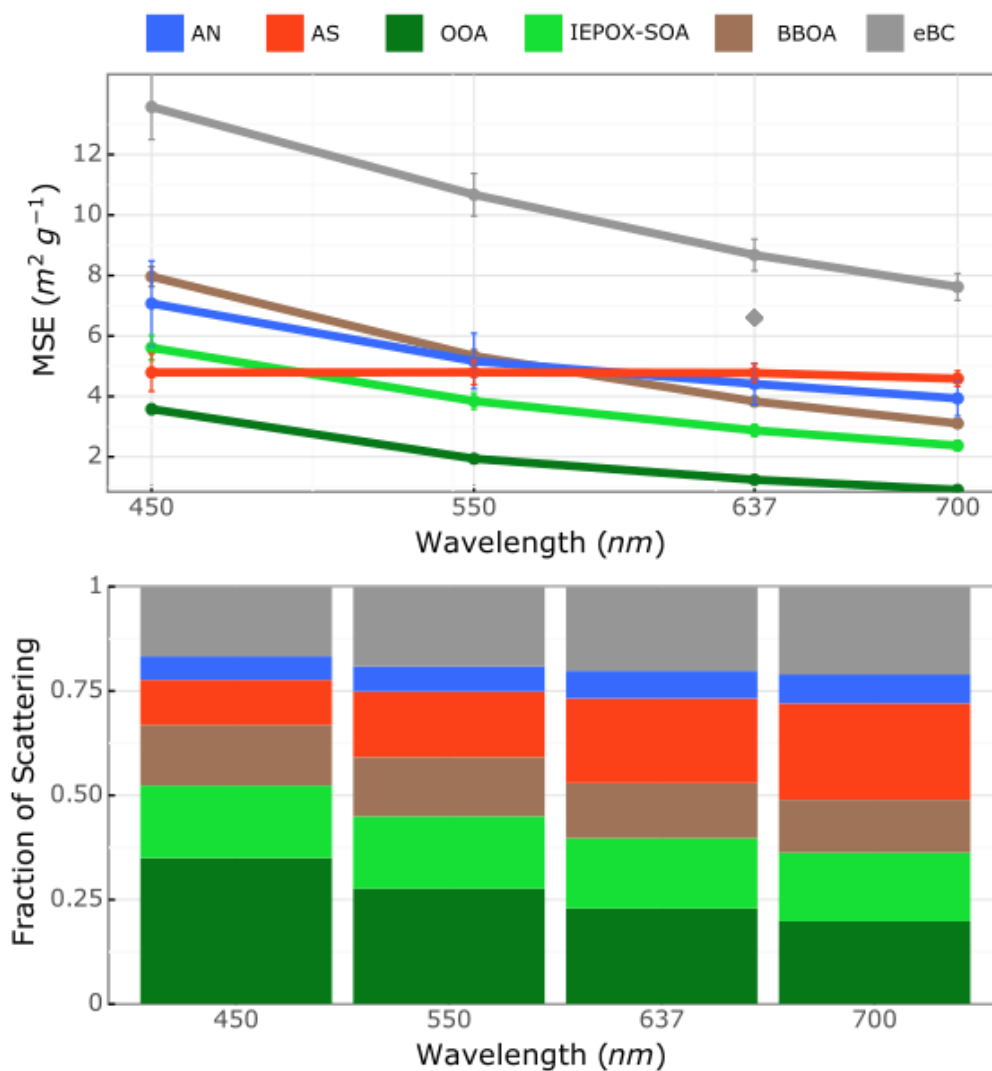
eBC	13.58±1.08	10.67±0.70	8.68±0.52	7.62±0.44	6.6	15.28±0.52
BBOA	7.96±0.33	5.33±0.21	3.83±0.16	3.10±0.13		
IEPOX-SOA	5.61±0.41	3.84±0.27	2.87±0.20	2.37±0.17		
OOA	3.58±0.15	1.94±0.10	1.24±0.07	0.90±0.06		
AS	4.79±0.62	4.79±0.41	4.77±0.30	4.58±0.25		
AN	7.07±1.41	5.17±0.92	4.41±0.68	3.93±0.58		

411
412
413
414



415

416 **Figure 6: Measured radiation scattering at 637 nm vs modeled scattering (MSE). The gray scale corresponds to the equivalent**
417 **mobility particle diameter for singly charged particles (D_{pg} , section 2.2). The blue line indicates a linear correlation.**

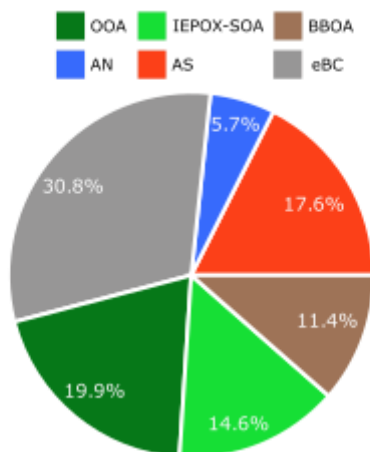


418

419 **Figure 7: a) Mass scattering efficiencies (MSE) for each chemical component (color lines) at each wavelength, where the dots are the**
420 **coefficients of the multi-linear regression, the bars are the standard errors, and the diamond shape is the value of absorption**
421 **efficiency of the eBC at 637 nm; and b) the fraction of scattering of each component at each wavelength, considering its mass fraction**
422 **to the total mass of submicrometer particles.**

423

424



425

426 **Figure 8: The relative contribution (%) of extinction coefficient (scattering + absorption) of each component considering its mass**
427 **fraction to the total mass of submicrometer particles.**

428 4 Conclusions

429 The results have shown that the submicrometer particle mass concentration during the dry season ($6.3 \pm 3.3 \mu\text{g m}^{-3}$), which is
430 about an order of magnitude higher than typically observed at this site during the wet season, is highly dominated by the
431 organic fraction ($77 \pm 5\%$). The organic aerosols were separated into 3 PMF statistical factors, identified as BBOA, OOA, and
432 IEPOX-SOA. The OOA, associated with highly processed and oxidized particles is the dominant factor ($51 \pm 6\%$ of the PM_{10}),
433 followed by IEPOX-SOA (isoprene SOA following a low-NO route, $17 \pm 5\%$), while the factor more directly associated with
434 fresh biomass burning emissions (BBOA) represents $9 \pm 5\%$ of PM_{10} .

435 The mean radiation scattering coefficient at 637 nm was $17 \pm 10 \text{ Mm}^{-1}$, and the mean absorption coefficient was $3 \pm 2 \text{ Mm}^{-1}$,
436 which are lower than the respective coefficients measured at sites much more impacted by the proximity to fresh forest fires
437 but exceed those observed during the wet season. The SSA of 0.87 ± 0.03 was elevated compared to values previously described
438 in the wet season, but generally in good agreement with SSA values of previous dry seasons. The mean scattering Angstrom
439 exponent was 1.76 ± 0.26 , surpassing the values previously measured during the wet season, likely due to the greater relative
440 proportion of smaller particles in the aerosol population measured in our study, compared to the primary biogenic aerosols,
441 Saharan dust and sea salt typical of the wet season in central Amazonia.

442 An MLR analysis of optical properties and different species/factors yielded the highest MSE for eBC in all wavelengths
443 followed by the BBOA and AN in the shorter wavelengths (450 and 550 nm), with the addition of AS in the longer wavelengths
444 (637 and 700 nm). Despite having a small mass contribution (6%), eBC dominated the MEE relative contribution (30.8%),
445 followed by the OOA (19.9%). The high MSE of eBC (and a calculated specific SSA of 0.57) is surprising, and more studies
446 concerning the chemical processing of those particles after their emission are needed in order to understand the processes



447 behind the outstanding efficiency of light scattering of this highly absorbing particle. A special focus should be given to the
448 role of aerosol coating in this process.

449 While previous studies show a significant contribution of organic particles to light absorption (brown carbon) our study shows
450 that the eBC can also have a significant contribution to light scattering. The quantification of the eBC contribution to light
451 scattering has the potential to improve models and decrease uncertainties in global radiative forcing estimations.

452 **Code availability**

453 **Data availability**

454 Data will be made available upon acceptance of the article.

455 **Author Contribution**

456 RS, JFB, and PA conceptualized and designed the methodology. RS performed the field measurements, with the support of
457 JFB. RS, JFB, SC, LVR and JDM applied the methodology. RS wrote the original draft, and all the authors discussed the
458 results and commented on the paper.

459

460 **Competing Interests**

461 Some authors are members of the editorial board of ACP.

462 **Acknowledgments**

463 We thank the Large-scale Biosphere-Atmosphere (LBA) project group and the Clima e Ambiente (CLIAMB) department at
464 Instituto Nacional de Pesquisas da Amazônia (INPA) for continuous support. The Brazil-UK Network for Investigation of
465 Amazonian Atmospheric Composition and Impacts on Climate (BUNIAACIC) project was funded by the UK Natural
466 Environment Research Council (NERC; grant NE/I030178/1) and FAPESP (2012/14437-9, 2013/05014-0). J. Brito was
467 funded by Fundação de Amparo à Pesquisa do Estado de São Paulo (FAPESP; project 2013/25058-1), by the Labex CaPPA
468 project, which is funded by the French National Research Agency (ANR) through the PIA (Programme d'Investissement
469 d'Avenir) under contract ANR-11-LABX-0005-01; the CLIMIBIO and ECRIN projects, all financed by the Regional Council
470 "Hauts-de-France" and the European Regional Development Fund (ERDF), and the COST COLOSSAL Action (CA16109).



471 L. Rizzo acknowledges the support of the Brazilian National Council for Research (CNPq, 304819/2022-0). We thank A.
472 Ribeiro, F. Morais, F. Jorge and S. Morais for technical and logistics support.

473

474 References

475 Alfara, M. R., Coe, H., Allan, J. D., Bower, K. N., Boudries, H., Canagaratna, M. R., Jimenez, J. L., Jayne, J. T., Garforth, A. a., Li, S.-M.
476 and Worsnop, D. R.: Characterization of urban and rural organic particulate in the Lower Fraser Valley using two Aerodyne Aerosol Mass
477 Spectrometers, *Atmos. Environ.*, 38(34), 5745–5758, doi:10.1016/j.atmosenv.2004.01.054, 2004.

478 Alfara, M. R., Prevot, A. S. H., Szidat, S., Sandradewi, J., Weimer, S., Lanz, V. a., Schreiber, D., Mohr, M. and Baltensperger, U.:
479 Identification of the Mass Spectral Signature of Organic Aerosols from Wood Burning Emissions, *Environ. Sci. Technol.*, 41(16), 5770–
480 5777, doi:10.1021/es062289b, 2007.

481 Allan, J. D., Morgan, W. T., Darbyshire, E., Flynn, M. J., Williams, P. I., Oram, D. E., Artaxo, P., Brito, J., Lee, J. D. and Coe, H.: Airborne
482 observations of IEPOX-derived isoprene SOA in the Amazon during SAMBBA, *Atmos. Chem. Phys.*, 14(20), 11393–11407,
483 doi:10.5194/acp-14-11393-2014, 2014.

484 Anderson, T. L. and Ogren, J. A.: Determining Aerosol Radiative Properties Using the TSI 3563 Integrating Nephelometer, *Aerosol Sci.*
485 *Technol.*, 29(1), 57–69, doi:10.1080/02786829808965551, 1998.

486 Andreae, M. O.: The Biosphere: Pilot or passenger on spaceship Earth?, *Contrib. to Glob. Chang. Res.*, (January 2001), 59–66, 2001.

487 Andreae, M. O., Acevedo, O. C., Araújo, A., Artaxo, P., Barbosa, C. G. G., Barbosa, H. M. J., Brito, J., Carbone, S., Chi, X., Cintra, B. B.
488 L., da Silva, N. F., Dias, N. L., Dias-Júnior, C. Q., Ditas, F., Ditz, R., Godoi, a. F. L., Godoi, R. H. M., Heimann, M., Hoffmann, T.,
489 Kesselmeier, J., Könemann, T., Krüger, M. L., Lavric, J. V., Manzi, a. O., Lopes, a. P., Martins, D. L., Mikhailov, E. F., Moran-Zuloaga,
490 D., Nelson, B. W., Nölscher, a. C., Santos Nogueira, D., Piedade, M. T. F., Pöhlker, C., Pöschl, U., Quesada, C. a., Rizzo, L. V., Ro, C.-U.,
491 Ruckteschler, N., Sá, L. D. a., de Oliveira Sá, M., Sales, C. B., dos Santos, R. M. N., Saturno, J., Schöngart, J., Sörgel, M., de Souza, C. M.,
492 de Souza, R. a. F., Su, H., Targhetta, N., Tóta, J., Trebs, I., Trumbore, S., van Eijck, A., Walter, D., Wang, Z., Weber, B., Williams, J.,
493 Winderlich, J., Wittmann, F., Wolff, S. and Yáñez-Serrano, a. M.: The Amazon Tall Tower Observatory (ATTO): overview of pilot
494 measurements on ecosystem ecology, meteorology, trace gases, and aerosols, *Atmos. Chem. Phys.*, 15(18), 10723–10776, doi:10.5194/acp-
495 15-10723-2015, 2015.

496 Aragão, L. E. O. C., Anderson, L. O., Lima, A. and Arai, E.: Fires in Amazonia, pp. 301–329., 2016.

497 Araújo, A. C., Nobre, A. D., Kruijt, B., Elbers, A., Dallarosa, R., Stefani, P., von Randow, C., Manzi, A. O., Culf, A. D., Gash, J. H. C.,
498 Valentini, R. and Kabat, P.: Comparative measurements of carbon dioxide fluxes from two nearby towers in a central Amazonian rainforest:
499 The Manaus LBA site, *J. Geophys. Res.*, 107(D20), doi:10.1029/2001JD000676, 2002.

500 Artaxo, P., Rizzo, L. V., Brito, J. F., Barbosa, H. M. J., Arana, A., Sena, E. T., Cirino, G. G., Bastos, W., Martin, S. T. and Andreae, M. O.:
501 Atmospheric aerosols in Amazonia and land use change: from natural biogenic to biomass burning conditions, *Faraday Discuss.*, 165, 203,
502 doi:10.1039/c3fd00052d, 2013.

503 Berenguer, E., Armenteras, D., Lees, A. C., Smith, C. C., Fearnside, P., Nascimento, N., Alencar, A., Almeida, C., Aragão, L. E. O., Barlow,
504 J., Bilbao, B., Brando, P. M., Bynoe, P., Finer, M., Flores, B. M., Jenkins, C. N., Silva Junior, C. H. L., Souza, C. and García-Villacorta, R.:
505 Chapter 19: Drivers and ecological impacts of deforestation and forest degradation., 2021.

506 Bond, T. C. and Bergstrom, R. W.: Light absorption by carbonaceous particles: An investigative review, *Aerosol Sci. Technol.*, 40(1), 27–
507 67, doi:10.1080/02786820500421521, 2006.

508 Brito, J., Rizzo, L. V., Morgan, W. T., Coe, H., Johnson, B., Haywood, J., Longo, K., Freitas, S., Andreae, M. O. and Artaxo, P.: Ground-
509 based aerosol characterization during the South American Biomass Burning Analysis (SAMBBA) field experiment, *Atmos. Chem. Phys.*,
510 14(22), 12069–12083, doi:10.5194/acp-14-12069-2014, 2014.



- 511 Brito, J., Freney, E., Dominutti, P., Borbon, A., Haslett, S. L., Batenburg, A. M., Colomb, A., Dupuy, R., Denjean, C., Burnet, F., Bourriane,
512 T., Deroubaix, A., Sellegri, K., Borrmann, S., Coe, H., Flamant, C., Knippertz, P. and Schwarzenboeck, A.: Assessing the role of
513 anthropogenic and biogenic sources on PM₁ over southern West Africa using aircraft measurements, *Atmos. Chem. Phys.*, 18, 757–772,
514 doi:10.5194/acp-18-757-2018, 2018.
- 515 Budisulistiorini, S. H., Canagaratna, M. R., Croteau, P. L., Marth, W. J., Baumann, K., Edgerton, E. S., Shaw, S. L., Knipping, E. M.,
516 Worsnop, D. R., Jayne, J. T., Gold, A. and Surratt, J. D.: Real-time continuous characterization of secondary organic aerosol derived from
517 isoprene epoxydiols in downtown Atlanta, Georgia, using the aerodyne aerosol chemical speciation monitor, *Environ. Sci. Technol.*, 47(11),
518 5686–5694, doi:10.1021/es400023n, 2013.
- 519 Caravan, R. L., Bannan, T. J., Winiberg, F. A. F., Khan, M. A. H., Rousso, A. C., Jasper, A. W., Worrall, S. D., Bacak, A., Artaxo, P., Brito,
520 J., Priestley, M., Allan, J. D., Coe, H., Ju, Y., Osborn, D. L., Hansen, N., Klippenstein, S. J., Shallcross, D. E., Taatjes, C. A. and Percival,
521 C. J.: Observational evidence for Criegee intermediate oligomerization reactions relevant to aerosol formation in the troposphere, *Nat.*
522 *Geosci.*, 1, doi:10.1038/s41561-023-01361-6, 2024.
- 523 Carbone, S., Saarikoski, S., Frey, A., Reyes, F., Reyes, P., Castillo, M., Gramsch, E., Oyola, P., Jayne, J., Worsnop, D. R. and Hillamo, R.:
524 Chemical Characterization of Submicron Aerosol Particles in Santiago de Chile, *Aerosol Air Qual. Res.*, 462–473,
525 doi:10.4209/aaqr.2012.10.0261, 2013.
- 526 Chen, G., Canonaco, F., Tobler, A., Aas, W., Alastuey, A., Allan, J., Atabakhsh, S., Aurela, M., Baltensperger, U., Bougiatioti, A., De Brito,
527 J. F., Ceburnis, D., Chazeanu, B., Chebaicheb, H., Daellenbach, K. R., Ehn, M., El Haddad, I., Eleftheriadis, K., Favez, O., Flentje, H., Font,
528 A., Fossum, K., Freney, E., Gini, M., Green, D. C., Heikkinen, L., Herrmann, H., Kalogridis, A.-C., Keernik, H., Lhotka, R., Lin, C., Lunder,
529 C., Maasikmets, M., Manousakas, M. I., Marchand, N., Marin, C., Marmureanu, L., Mihalopoulos, N., Močnik, G., Nęcki, J., O’Dowd, C.,
530 Ovadnevaite, J., Peter, T., Petit, J.-E., Pikridas, M., Matthew Platt, S., Pokorná, P., Poulain, L., Priestman, M., Riffault, V., Rinaldi, M.,
531 Róžański, K., Schwarz, J., Sciare, J., Simon, L., Skiba, A., Slowik, J. G., Sosedova, Y., Stavroulas, I., Styszko, K., Teinmaa, E., Timonen,
532 H., Tremper, A., Vasilescu, J., Via, M., Vodička, P., Wiedensohler, A., Zografou, O., Cruz Minguillón, M. and Prévôt, A. S. H.: European
533 aerosol phenomenology – 8: Harmonised source apportionment of organic aerosol using 22 Year-long ACSM/AMS datasets, *Environ. Int.*,
534 166(May), 107325, doi:10.1016/j.envint.2022.107325, 2022.
- 535 Chen, Q., Farmer, D. K., Schneider, J., Zorn, S. R., Heald, C. L., Karl, T. G., Guenther, a., Allan, J. D., Robinson, N., Coe, H., Kimmel, J.
536 R., Pauliquevis, T., Borrmann, S., Pöschl, U., Andreae, M. O., Artaxo, P., Jimenez, J. L. and Martin, S. T.: Mass spectral characterization of
537 submicron biogenic organic particles in the Amazon Basin, *Geophys. Res. Lett.*, 36(20), L20806, doi:10.1029/2009GL039880, 2009.
- 538 Chen, Q., Farmer, D. K., Rizzo, L. V., Pauliquevis, T., Kuwata, M., Karl, T. G., Guenther, a., Allan, J. D., Coe, H., Andreae, M. O., Pöschl,
539 U., Jimenez, J. L., Artaxo, P. and Martin, S. T.: Submicron particle mass concentrations and sources in the Amazonian wet season (AMAZE-
540 08), *Atmos. Chem. Phys.*, 15(7), 3687–3701, doi:10.5194/acp-15-3687-2015, 2015.
- 541 Cubison, M. J., Ortega, a. M., Hayes, P. L., Farmer, D. K., Day, D., Lechner, M. J., Brune, W. H., Apel, E., Diskin, G. S., Fisher, J. a.,
542 Fuelberg, H. E., Hecobian, a., Knapp, D. J., Mikoviny, T., Riemer, D., Sachse, G. W., Sessions, W., Weber, R. J., Weinheimer, a. J.,
543 Wisthaler, a. and Jimenez, J. L.: Effects of aging on organic aerosol from open biomass burning smoke in aircraft and laboratory studies,
544 *Atmos. Chem. Phys.*, 11(23), 12049–12064, doi:10.5194/acp-11-12049-2011, 2011.
- 545 Darbyshire, E., Morgan, W. T., Allan, J. D., Liu, D., Flynn, M. J., Dorsey, J. R., O’Shea, S. J., Lowe, D., Szpek, K., Marengo, F., Johnson,
546 B. T., Bauguutte, S., Haywood, J. M., Brito, J. F., Artaxo, P., Longo, K. M. and Coe, H.: The vertical distribution of biomass burning pollution
547 over tropical South America from aircraft in situ measurements during SAMBBA, *Atmos. Chem. Phys.*, 19(9), 5771–5790, doi:10.5194/acp-
548 19-5771-2019, 2019.
- 549 Davidson, E. a, de Araújo, A. C., Artaxo, P., Balch, J. K., Brown, I. F., C Bustamante, M. M., Coe, M. T., DeFries, R. S., Keller, M., Longo,
550 M., Munger, J. W., Schroeder, W., Soares-Filho, B. S., Souza, C. M. and Wofsy, S. C.: The Amazon basin in transition., *Nature*, 481(7381),
551 321–8, doi:10.1038/nature10717, 2012.
- 552 Denjean, C., Brito, J., Libois, Q., Mallet, M., Bourriane, T., Burnet, F., Dupuy, R., Flamant, C. and Knippertz, P.: Unexpected Biomass
553 Burning Aerosol Absorption Enhancement Explained by Black Carbon Mixing State, *Geophys. Res. Lett.*, 47(19), 1–11,
554 doi:10.1029/2020GL089055, 2020.
- 555 Draxler, R. R. and Hess, G. D.: An overview of the HYSPLIT₄ modelling system for trajectories, dispersion and deposition, *Aust. Meteorol.*



- 556 Mag., 47(4), 295–308, 1998.
- 557 F. G. Assis, L. F., Ferreira, K. R., Vinhas, L., Maurano, L., Almeida, C., Carvalho, A., Rodrigues, J., Maciel, A. and Camargo, C.:
558 TerraBrasilis: A Spatial Data Analytics Infrastructure for Large-Scale Thematic Mapping, *ISPRS Int. J. Geo-Information*, 8(11), 513,
559 doi:10.3390/ijgi8110513, 2019.
- 560 Fisch, G., Tota, J., Machado, L. a. T., Silva Dias, M. a. F., da F. Lyra, R. F., Nobre, C. a., Dolman, a. J. and Gash, J. H. C.: The convective
561 boundary layer over pasture and forest in Amazonia, *Theor. Appl. Climatol.*, 78(1–3), 47–59, doi:10.1007/s00704-004-0043-x, 2004.
- 562 Flores, B. M., Montoya, E., Sakschewski, B., Nascimento, N., Staal, A., Betts, R. A., Levis, C., Lapola, D. M., Esquivel-Muelbert, A.,
563 Jakovac, C., Nobre, C. A., Oliveira, R. S., Borma, L. S., Nian, D., Boers, N., Hecht, S. B., ter Steege, H., Arieira, J., Lucas, I. L., Berenguer,
564 E., Marengo, J. A., Gatti, L. V., Mattos, C. R. C. and Hirota, M.: Critical transitions in the Amazon forest system, *Nature*, 626(7999), 555–
565 564, doi:10.1038/s41586-023-06970-0, 2024.
- 566 Forster, P. M., Storelvmo, T., Armour, K., Collins, W., Dufresne, J.-L., Frame, D., Lunt, D. J., Mauritsen, T., Palmer, M. D., Watanabe, M.,
567 Wild, M. and Zhang, H.: The Earth’s Energy Budget, Climate Feedbacks and Climate Sensitivity, in *Climate Change 2021 – The Physical
568 Science Basis. Contribution of Working Group I to the Sixth Assessment Report of the Intergovernmental Panel on Climate Change [Masson-
569 Delmotte, V., P. Zhai, A. Pirani, S.L. Connors, C. Pean, S. Berger, N. Caud, Y. Chen, pp. 923–1054, Cambridge University Press, Cambridge
570 and New York., 2021.*
- 571 Fuzzi, S., Decesari, S., Facchini, M. C., Cavalli, F., Emblico, L., Mircea, M., Andreae, M. O., Trebs, I., Hoffer, A., Guyon, P., Artaxo, P.,
572 Rizzo, L. V., Lara, L. L., Pauliquevis, T., Maenhaut, W., Raes, N., Chi, X., Mayol-Bracero, O. L., Soto-García, L. L., Claeys, M., Kourchev,
573 I., Rissler, J., Swietlicki, E., Tagliavini, E., Schkolnik, G., Falkovich, A. H., Rudich, Y., Fisch, G. and Gatti, L. V.: Overview of the inorganic
574 and organic composition of size-segregated aerosol in Rondônia, Brazil, from the biomass-burning period to the onset of the wet season, *J.
575 Geophys. Res.*, 112(D1), D01201, doi:10.1029/2005JD006741, 2007.
- 576 Hand, J. L. and Malm, W. C.: Review of aerosol mass scattering efficiencies from ground-based measurements since 1990, *J. Geophys. Res.*
577 *Atmos.*, 112(16), doi:10.1029/2007JD008484, 2007.
- 578 He, C., Liou, K. N., Takano, Y., Zhang, R., Levy Zamora, M., Yang, P., Li, Q. and Leung, L. R.: Variation of the radiative properties during
579 black carbon aging: Theoretical and experimental intercomparison, *Atmos. Chem. Phys.*, 15(20), 11967–11980, doi:10.5194/acp-15-11967-
580 2015, 2015.
- 581 Holanda, B. A., Pöhlker, M. L., Walter, D., Saturno, J., Sörgel, M., Ditas, J., Ditas, F., Schulz, C., Franco, M. A., Wang, Q., Donth, T.,
582 Artaxo, P., Barbosa, H. M. J., Borrmann, S., Braga, R., Brito, J., Cheng, Y., Dollner, M., Kaiser, J. W., Klimach, T., Knote, C., Krüger, O.
583 O., Fütterer, D., Lavrič, J. V., Ma, N., Machado, L. A. T., Ming, J., Morais, F. G., Paulsen, H., Sauer, D., Schlager, H., Schneider, J., Su, H.,
584 Weinzierl, B., Walser, A., Wendisch, M., Ziereis, H., Zöger, M., Pöschl, U., Andreae, M. O. and Pöhlker, C.: Influx of African biomass
585 burning aerosol during the Amazonian dry season through layered transatlantic transport of black carbon-rich smoke, *Atmos. Chem. Phys.*,
586 20(8), 4757–4785, doi:10.5194/acp-20-4757-2020, 2020.
- 587 Holanda, B. A., Franco, M. A., Walter, D., Artaxo, P., Carbone, S., Cheng, Y., Chowdhury, S., Ditas, F., Gysel-Beer, M., Klimach, T.,
588 Krempfer, L. A., Krüger, O. O., Lavric, J. V., Lelieveld, J., Ma, C., Machado, L. A. T., Modini, R. L., Morais, F. G., Pozzer, A., Saturno, J.,
589 Su, H., Wendisch, M., Wolff, S., Pöhlker, M. L., Andreae, M. O., Pöschl, U. and Pöhlker, C.: African biomass burning affects aerosol cycling
590 over the Amazon, *Commun. Earth Environ.*, 4(1), 1–15, doi:10.1038/s43247-023-00795-5, 2023.
- 591 Hu, W., Palm, B. B., Day, D. A., Campuzano-Jost, P., Krechmer, J. E., Peng, Z., De Sa Suzane, S., Martin, S. T., Alexander, M. L., Baumann,
592 K., Hacker, L., Kiendler-Scharr, A., Koss, A. R., De Gouw, J. A., Goldstein, A. H., Seco, R., Sjostedt, S. J., Park, J. H., Guenther, A. B.,
593 Kim, S., Canonaco, F., Prévôt, A. S. H., Brune, W. H. and Jimenez, J. L.: Volatility and lifetime against OH heterogeneous reaction of
594 ambient isoprene-epoxydiols-derived secondary organic aerosol (IEPOX-SOA), *Atmos. Chem. Phys.*, 16(18), 11563–11580,
595 doi:10.5194/acp-16-11563-2016, 2016.
- 596 Hu, W. W., Campuzano-Jost, P., Palm, B. B., Day, D. A., Ortega, A. M., Hayes, P. L., Krechmer, J. E., Chen, Q., Kuwata, M., Liu, Y. J., de
597 Sá, S. S., Martin, S. T., Hu, M., Budisulistiorini, S. H., Riva, M., Surratt, J. D., St. Clair, J. M., Isaacman-Van Wertz, G., Yee, L. D.,
598 Goldstein, A. H., Carbone, S., Artaxo, P., de Gouw, J. A., Koss, A., Wisthaler, A., Mikoviny, T., Karl, T., Kaser, L., Jud, W., Hansel, A.,
599 Docherty, K. S., Robinson, N. H., Coe, H., Allan, J. D., Canagaratna, M. R., Paulot, F. and Jimenez, J. L.: Characterization of a real-time
600 tracer for Isoprene Epoxydiols-derived Secondary Organic Aerosol (IEPOX-SOA) from aerosol mass spectrometer measurements, *Atmos.*



- 601 Chem. Phys. Discuss., 15(8), 11223–11276, doi:10.5194/acpd-15-11223-2015, 2015.
- 602 Instituto Nacional de Pesquisas Espaciais: Portal do Monitoramento de Queimadas e Incêndios Florestais, [online] Available from:
603 http://terrabrazilis.dpi.inpe.br/queimadas/situacao-actual/estatisticas/estatisticas_estados/#footer, 2024.
- 604 Jimenez, J. L., Canagaratna, M. R., Donahue, N. M., Prevot, a. S. H., Zhang, Q., Kroll, J. H., DeCarlo, P. F., Allan, J. D., Coe, H., Ng, N.
605 L., Aiken, a. C., Docherty, K. S., Ulbrich, I. M., Grieshop, a. P., Robinson, a. L., Duplissy, J., Smith, J. D., Wilson, K. R., Lanz, V. a.,
606 Hueglin, C., Sun, Y. L., Tian, J., Laaksonen, A., Raatikainen, T., Rautiainen, J., Vaattovaara, P., Ehn, M., Kulmala, M., Tomlinson, J. M.,
607 Collins, D. R., Cubison, M. J., Dunlea, J., Huffman, J. a., Onasch, T. B., Alfarra, M. R., Williams, P. I., Bower, K., Kondo, Y., Schneider,
608 J., Drewnick, F., Borrmann, S., Weimer, S., Demerjian, K., Salcedo, D., Cottrell, L., Griffin, R., Takami, A., Miyoshi, T., Hatakeyama, S.,
609 Shimono, A., Sun, J. Y., Zhang, Y. M., Dzepina, K., Kimmel, J. R., Sueper, D., Jayne, J. T., Herndon, S. C., Trimborn, a. M., Williams, L.
610 R., Wood, E. C., Middlebrook, a. M., Kolb, C. E., Baltensperger, U. and Worsnop, D. R.: Evolution of Organic Aerosols in the Atmosphere,
611 *Science* (80-.), 326(5959), 1525–1529, doi:10.1126/science.1180353, 2009.
- 612 Kleinman, L. I., Sedlacek, A. J., Adachi, K., Buseck, P. R., Collier, S., Dubey, M. K., Hodshire, A. L., Lewis, E., Onasch, T. B., Pierce, J.
613 R., Shilling, J., Springston, S. R., Wang, J., Zhang, Q., Zhou, S. and Yokelson, R. J.: Rapid evolution of aerosol particles and their optical
614 properties downwind of wildfires in the western US, *Atmos. Chem. Phys.*, 20(21), 13319–13341, doi:10.5194/acp-20-13319-2020, 2020.
- 615 Kroll, J. H., Ng, N. L., Murphy, S. M., Flagan, R. C. and Seinfeld, J. H.: Secondary Organic Aerosol Formation from Isoprene
616 Photooxidation, *Environ. Sci. Technol.*, 40(6), 1869–1877, doi:10.1021/es0524301, 2006.
- 617 Kuhn, U., Ganzeveld, L., Thielmann, A., Dindorf, T., Schebeske, G., Welling, M., Sciare, J., Roberts, G., Meixner, F. X., Kesselmeier, J.,
618 Lelieveld, J., Kolle, O., Ciccioli, P., Lloyd, J., Trentmann, J., Artaxo, P. and Andreae, M. O.: Impact of Manaus City on the Amazon Green
619 Ocean atmosphere: Ozone production, precursor sensitivity and aerosol load, *Atmos. Chem. Phys.*, 10(19), 9251–9282, doi:10.5194/acp-10-
620 9251-2010, 2010.
- 621 Laskin, A., Laskin, J. and Nizkorodov, S. A.: Chemistry of Atmospheric Brown Carbon, *Chem. Rev.*, 115(10), 4335–4382,
622 doi:10.1021/cr5006167, 2015.
- 623 Lee, T., Sullivan, A. P., Mack, L., Jimenez, J. L., Kreidenweis, S. M., Onasch, T. B., Worsnop, D. R., Malm, W., Wold, C. E., Hao, W. M.
624 and Collett, J. L.: Chemical Smoke Marker Emissions During Flaming and Smoldering Phases of Laboratory Open Burning of Wildland
625 Fuels, *Aerosol Sci. Technol.*, 44(9), i–v, doi:10.1080/02786826.2010.499884, 2010.
- 626 Lin, Y., Zhang, Z., Docherty, K. S., Zhang, H., Budisulistiorini, S. H., Rubitschun, C. L., Shaw, S. L., Knipping, E. M., Edgerton, E. S.,
627 Kleindienst, T. E., Gold, A. and Surratt, J. D.: Isoprene Epoxydiols as Precursors to Secondary Organic Aerosol Formation : Acid-Catalyzed
628 Reactive Uptake Studies with Authentic Compounds, , 250–258, 2012.
- 629 Luo, J., Zhang, Y. and Zhang, Q.: The Ångström Exponent and Single-Scattering Albedo of Black Carbon: Effects of Different Coating
630 Materials, *Atmosphere (Basel)*, 11(10), 1103, doi:10.3390/atmos11101103, 2020.
- 631 Malm, W. C., Day, D. E., Carrico, C., Kreidenweis, S. M., Collett, J. L., McMeeking, G., Lee, T., Carrillo, J. and Schichtel, B.:
632 Intercomparison and closure calculations using measurements of aerosol species and optical properties during the Yosemite aerosol
633 characterization study, *J. Geophys. Res. D Atmos.*, 110(14), 1–21, doi:10.1029/2004JD005494, 2005.
- 634 Marais, E. A., Jacob, D. J., Jimenez, J. L., Campuzano-Jost, P., Day, D. A., Hu, W., Krechmer, J., Zhu, L., Kim, P. S., Miller, C. C., Fisher,
635 J. A., Travis, K., Yu, K., Hanisco, T. F., Wolfe, G. M., Arkinson, H. L., Pye, H. O. T., Froyd, K. D., Liao, J. and McNeill, V. F.: Aqueous-
636 phase mechanism for secondary organic aerosol formation from isoprene: application to the southeast United States and co-benefit of SO₂
637 emission controls, *Atmos. Chem. Phys.*, 16(3), 1603–1618, doi:10.5194/acp-16-1603-2016, 2016.
- 638 Marengo, J. A., Liebmann, B., Kousky, V. E., Filizola, N. P. and Wainer, I. C.: Onset and End of the Rainy Season in the Brazilian Amazon
639 Basin, *J. Clim.*, 14(5), 833–852, doi:10.1175/1520-0442(2001)014<0833:OAEOTR>2.0.CO;2, 2001.
- 640 Martin, S. T., Andreae, M. O., Althausen, D., Artaxo, P., Baars, H., Borrmann, S., Chen, Q., Farmer, D. K., Guenther, a., Gunthe, S. S.,
641 Jimenez, J. L., Karl, T., Longo, K., Manzi, a., Müller, T., Pauliquevis, T., Petters, M. D., Prenni, a. J., Pöschl, U., Rizzo, L. V., Schneider,
642 J., Smith, J. N., Swietlicki, E., Tota, J., Wang, J., Wiedensohler, a. and Zorn, S. R.: An overview of the Amazonian Aerosol Characterization
643 Experiment 2008 (AMAZE-08), *Atmos. Chem. Phys.*, 10(23), 11415–11438, doi:10.5194/acp-10-11415-2010, 2010a.



- 644 Martin, S. T., Andreae, M. O., Artaxo, P., Baumgardner, D., Chen, Q., Goldstein, A. H., Guenther, A., Heald, C. L., Mayol-Bracero, O. L.,
645 McMurry, P. H., Pauliquevis, T., Pöschl, U., Prather, K. A., Roberts, G. C., Saleska, S. R., Silva Dias, M. A., Spracklen, D. V., Swietlicki,
646 E. and Trebs, I.: Sources and properties of Amazonian aerosol particles, *Rev. Geophys.*, 48(2), RG2002, doi:10.1029/2008RG000280, 2010b.
- 647 Martin, S. T., Artaxo, P., Machado, L. A. T., Manzi, A. O., Souza, R. A. F., Schumacher, C., Wang, J., Andreae, M. O., Barbosa, H. M. J.,
648 Fan, J., Fisch, G., Goldstein, A. H., Guenther, A., Jimenez, J. L., Pöschl, U., Silva Dias, M. A., Smith, J. N. and Wendisch, M.: Introduction:
649 Observations and Modeling of the Green Ocean Amazon (GoAmazon2014/5), *Atmos. Chem. Phys. Discuss.*, 15(21), 30175–30210,
650 doi:10.5194/acpd-15-30175-2015, 2015.
- 651 Middlebrook, A. M., Bahreini, R., Jimenez, J. L. and Canagaratna, M. R.: Evaluation of Composition-Dependent Collection Efficiencies for
652 the Aerodyne Aerosol Mass Spectrometer using Field Data, *Aerosol Sci. Technol.*, 46(3), 258–271, doi:10.1080/02786826.2011.620041,
653 2012.
- 654 Müller, T., Henzing, J. S., De Leeuw, G., Wiedensohler, A., Alastuey, A., Angelov, H., Bizjak, M., Collaud Coen, M., Engström, J. E.,
655 Gruening, C., Hillamo, R., Hoffer, A., Imre, K., Ivanow, P., Jennings, G., Sun, J. Y., Kalivitis, N., Karlsson, H., Komppula, M., Laj, P., Li,
656 S. M., Lunder, C., Marinoni, A., Martins Dos Santos, S., Moerman, M., Nowak, A., Ogren, J. A., Petzold, A., Pichon, J. M., Rodriguez, S.,
657 Sharma, S., Sheridan, P. J., Teinilä, K., Tuch, T., Viana, M., Virkkula, A., Weingartner, E., Wilhelm, R. and Wang, Y. Q.: Characterization
658 and intercomparison of aerosol absorption photometers: Result of two intercomparison workshops, *Atmos. Meas. Tech.*, 4(2), 245–268,
659 doi:10.5194/amt-4-245-2011, 2011.
- 660 Myhre, G., Samset, B. H., Schulz, M., Balkanski, Y., Bauer, S., Bernsten, T. K., Bian, H., Bellouin, N., Chin, M., Diehl, T., Easter, R. C.,
661 Feichter, J., Ghan, S. J., Hauglustaine, D., Iversen, T., Kinne, S., Kirkevåg, A., Lamarque, J. F., Lin, G., Liu, X., Lund, M. T., Luo, G., Ma,
662 X., Van Noije, T., Penner, J. E., Rasch, P. J., Ruiz, A., Seland, Skeie, R. B., Stier, P., Takemura, T., Tsigaridis, K., Wang, P., Wang, Z., Xu,
663 L., Yu, H., Yu, F., Yoon, J. H., Zhang, K., Zhang, H. and Zhou, C.: Radiative forcing of the direct aerosol effect from AeroCom Phase II
664 simulations, *Atmos. Chem. Phys.*, 13(4), 1853–1877, doi:10.5194/acp-13-1853-2013, 2013.
- 665 Nah, T., Xu, L., Osborne-Benthaus, K. A., White, S. M., France, S. and Lee Ng, N.: Mixing order of sulfate aerosols and isoprene epoxydiols
666 affects secondary organic aerosol formation in chamber experiments, *Atmos. Environ.*, 217(September),
667 doi:10.1016/j.atmosenv.2019.116953, 2019.
- 668 Nascimento, J. P., Bela, M. M., Meller, B. B., Banducci, A. L., Rizzo, L. V., Liduvino Vara-Vela, A., Barbosa, H. M. J., Gomes, H., Rafee,
669 S. A. A., Franco, M. A., Carbone, S., Cirino, G. G., Souza, R. A. F., Mckeen, S. A. and Artaxo, P.: Aerosols from anthropogenic and biogenic
670 sources and their interactions—modeling aerosol formation, optical properties, and impacts over the central Amazon basin, *Atmos. Chem.*
671 *Phys.*, 21(9), 6755–6779, doi:10.5194/acp-21-6755-2021, 2021.
- 672 Ng, N. L., Herndon, S. C., Trimborn, A., Canagaratna, M. R., Croteau, P. L., Onasch, T. B., Sueper, D., Worsnop, D. R., Zhang, Q., Sun, Y.
673 L. and Jayne, J. T.: An Aerosol Chemical Speciation Monitor (ACSM) for routine monitoring of the composition and mass concentrations
674 of ambient aerosol, *Aerosol Sci. Technol.*, 45(7), 780–794, doi:10.1080/02786826.2011.560211, 2011.
- 675 Paatero, P. and Tapper, U.: Positive Matrix Factorization: a non-negative factor model with optimal utilization of error estimates of data
676 values, *Environmetrics*, 5, 111–126, 1994.
- 677 Palácios, R. da S., Romera, K. S., Curado, L. F. A., Banga, N. M., Rothmund, L. D., Sallo, F. da S., Morais, D., Santos, A. C. A., Moraes,
678 T. J., Morais, F. G., Landulfo, E., Franco, M. A. de M., Kuhnén, I. A., Marques, J. B., Nogueira, J. de S., Júnior, L. C. G. D. V. and Rodrigues,
679 T. R.: Long term analysis of optical and radiative properties of aerosols in the amazon basin, *Aerosol Air Qual. Res.*, 20(1), 139–154,
680 doi:10.4209/aaqr.2019.04.0189, 2020.
- 681 Paredes-Miranda, G., Arnott, W. P., Jimenez, J. L., Aiken, A. C., Gaffney, J. S. and Marley, N. A.: Primary and secondary contributions to
682 aerosol light scattering and absorption in Mexico City during the MILAGRO 2006 campaign, *Atmos. Chem. Phys.*, 9(11), 3721–3730,
683 doi:10.5194/acp-9-3721-2009, 2009.
- 684 Petzold, A., Schloesser, H., Sheridan, P. J., Arnott, W. P., Ogren, J. A. and Virkkula, A.: Evaluation of Multiangle Absorption Photometry
685 for Measuring Aerosol Light Absorption, *Aerosol Sci. Technol.*, 39(1), 40–51, doi:10.1080/027868290901945, 2005.
- 686 Pohlker, C., Wiedemann, K. T., Sinha, B., Shiraiwa, M., Gunthe, S. S., Smith, M., Su, H., Artaxo, P., Chen, Q., Cheng, Y., Elbert, W., Gilles,
687 M. K., Kilcoyne, A. L. D., Moffet, R. C., Weigand, M., Martin, S. T., Pöschl, U., Andreae, M. O., Pöhlker, C., Wiedemann, K. T., Sinha,



- 688 B., Shiraiwa, M., Gunthe, S. S., Smith, M., Su, H., Artaxo, P., Chen, Q., Cheng, Y., Elbert, W., Gilles, M. K., Kilcoyne, A. L. D., Moffet,
689 R. C., Weigand, M., Martin, S. T., Pöschl, U. and Andreae, M. O.: Biogenic potassium salt particles as seeds for secondary organic aerosol
690 in the Amazon., *Science*, 337(6098), 1075–8, doi:10.1126/science.1223264, 2012.
- 691 Pöhlker, M. L., Pöhlker, C., Ditas, F., Klimach, T., De Angelis, I. H., Araújo, A., Brito, J., Carbone, S., Cheng, Y., Chi, X., Ditz, R., Gunthe,
692 S. S., Kesselmeier, J., Könemann, T., Lavrič, J. V., Martin, S. T., Mikhailov, E., Moran-Zuloaga, D., Rose, D., Saturno, J., Su, H., Thalman,
693 R., Walter, D., Wang, J., Wolff, S., Barbosa, H. M. J., Artaxo, P., Andreae, M. O. and Pöschl, U.: Long-term observations of cloud
694 condensation nuclei in the Amazon rain forest - Part 1: Aerosol size distribution, hygroscopicity, and new model parametrizations for CCN
695 prediction, *Atmos. Chem. Phys.*, 16(24), 15709–15740, doi:10.5194/acp-16-15709-2016, 2016.
- 696 Pöhlker, M. L., Ditas, F., Saturno, J., Klimach, T., Hrabě De Angelis, I., Araújo, A. C., Brito, J., Carbone, S., Cheng, Y., Chi, X., Ditz, R.,
697 Gunthe, S. S., Holanda, B. A., Kandler, K., Kesselmeier, J., Könemann, T., Krüger, O. O., Lavric, J. V., Martin, S. T., Mikhailov, E., Moran-
698 Zuloaga, D., Rizzo, L. V., Rose, D., Su, H., Thalman, R., Walter, D., Wang, J., Wolff, S., Barbosa, H. M. J., Artaxo, P., Andreae, M. O.,
699 Pöschl, U. and Pöhlker, C.: Long-term observations of cloud condensation nuclei over the Amazon rain forest - Part 2: Variability and
700 characteristics of biomass burning, long-range transport, and pristine rain forest aerosols, *Atmos. Chem. Phys.*, 18(14), 10289–10331,
701 doi:10.5194/acp-18-10289-2018, 2018.
- 702 Ponczek, M., Franco, M. A., Carbone, S., Rizzo, L. V., Monteiro dos Santos, D., Morais, F. G., Duarte, A., Barbosa, H. M. J. and Artaxo,
703 P.: Linking the chemical composition and optical properties of biomass burning aerosols in Amazonia, *Environ. Sci. Atmos.*, 2(2), 252–269,
704 doi:10.1039/d1ea00055a, 2021.
- 705 Pöschl, U., Martin, S. T., Sinha, B., Chen, Q., Gunthe, S. S., Huffman, J. A., Borrmann, S., Farmer, D. K., Garland, R. M., Helas, G.,
706 Jimenez, J. L., King, S. M., Manzi, A., Mikhailov, E., Pauliquevis, T., Petters, M. D., Prenni, A. J., Roldin, P., Rose, D., Schneider, J., Su,
707 H., Zorn, S. R., Artaxo, P. and Andreae, M. O.: Rainforest Aerosols as Biogenic Nuclei of Clouds and Precipitation in the Amazon, *Science*
708 (80-.), 329(5998), 1513–1516, doi:10.1126/science.1191056, 2010.
- 709 Reid, J. S., Koppmann, R., Eck, T. F. and Eleuterio, D. P.: A review of biomass burning emissions part II: intensive physical properties of
710 biomass burning particles, *Atmos. Chem. Phys.*, 5(3), 799–825, doi:10.5194/acp-5-799-2005, 2005.
- 711 Rizzo, L. V., Artaxo, P., Müller, T., Wiedensohler, A., Paixão, M., Cirino, G. G., Arana, A., Swietlicki, E., Roldin, P., Fors, E. O.,
712 Wiedemann, K. T., Leal, L. S. M. and Kulmala, M.: Long term measurements of aerosol optical properties at a primary forest site in
713 Amazonia, *Atmos. Chem. Phys.*, 13(5), 2391–2413, doi:10.5194/acp-13-2391-2013, 2013.
- 714 de Sá, S. S., Palm, B. B., Campuzano-Jost, P., Day, D. A., Newburn, M. K., Hu, W., Isaacman-VanWertz, G., Yee, L. D., Thalman, R.,
715 Brito, J., Carbone, S., Artaxo, P., Goldstein, A. H., Manzi, A. O., Souza, R. A. F., Mei, F., Shilling, J. E., Springston, S. R., Wang, J., Surratt,
716 J. D., Alexander, M. L., Jimenez, J. L. and Martin, S. T.: Influence of urban pollution on the production of organic particulate matter from
717 isoprene epoxydiols in central Amazonia, *Atmos. Chem. Phys.*, 17(11), 6611–6629, doi:10.5194/acp-17-6611-2017, 2017.
- 718 de Sá, S. S., Palm, B. B., Campuzano-Jost, P., Day, D. A., Hu, W., Isaacman-VanWertz, G., Yee, L. D., Brito, J., Carbone, S., Ribeiro, I.,
719 O., Cirino, G. G., Liu, Y., Thalman, R., Sedlacek, A., Funk, A., Schumacher, C., Shilling, J. E., Schneider, J., Artaxo, P., Goldstein, A. H.,
720 Souza, R. A. F., Wang, J., McKinney, K. A., Barbosa, H., Alexander, M. L., Jimenez, J. L. and Martin, S. T.: Urban influence on the
721 concentration and composition of submicron particulate matter in central Amazonia, *Atmos. Chem. Phys.*, 18(16), 12185–12206,
722 doi:10.5194/acp-18-12185-2018, 2018.
- 723 de Sá, S. S., Rizzo, L. V., Palm, B. B., Campuzano-Jost, P., Day, D. A., Yee, L. D., Wernis, R., Isaacman-VanWertz, G., Brito, J., Carbone,
724 S., Liu, Y. J., Sedlacek, A., Springston, S., Goldstein, A. H., Barbosa, H. M. J., Alexander, M. L., Artaxo, P., Jimenez, J. L. and Martin, S.
725 T.: Contributions of biomass-burning, urban, and biogenic emissions to the concentrations and light-absorbing properties of particulate
726 matter in central Amazonia during the dry season, *Atmos. Chem. Phys.*, 19(12), 7973–8001, doi:10.5194/acp-19-7973-2019, 2019.
- 727 Saturno, J., Ditas, F., De Vries, M. P., Holanda, B. A., Pöhlker, M. L., Carbone, S., Walter, D., Bobrowski, N., Brito, J., Chi, X., Gutmann,
728 A., De Angelis, I. H., Machado, L. A. T., Moran-Zuloaga, D., Rüdiger, J., Schneider, J., Schulz, C., Wang, Q., Wendisch, M., Artaxo, P.,
729 Wagner, T., Pöschl, U., Andreae, M. O. and Pöhlker, C.: African volcanic emissions influencing atmospheric aerosols over the Amazon rain
730 forest, *Atmos. Chem. Phys.*, 18(14), 10391–10405, doi:10.5194/acp-18-10391-2018, 2018a.
- 731 Saturno, J., Holanda, B. A., Pöhlker, C., Ditas, F., Wang, Q., Moran-Zuloaga, D., Brito, J., Carbone, S., Cheng, Y., Chi, X., Ditas, J.,
732 Hoffmann, T., Hrabě De Angelis, I., Könemann, T., Lavrič, J. V., Ma, N., Ming, J., Paulsen, H., Pöhlker, M. L., Rizzo, L. V., Schlag, P.,



- 733 Su, H., Walter, D., Wolff, S., Zhang, Y., Artaxo, P., Pöschl, U. and Andreae, M. O.: Black and brown carbon over central Amazonia: Long-
734 term aerosol measurements at the ATTO site, *Atmos. Chem. Phys.*, 18(17), 12817–12843, doi:10.5194/acp-18-12817-2018, 2018b.
- 735 Schuster, G. L., Dubovik, O. and Holben, B. N.: Angstrom exponent and bimodal aerosol size distributions, *J. Geophys. Res. Atmos.*,
736 111(D7), D07207, doi:10.1029/2005JD006328, 2006.
- 737 Sena, E. T., Artaxo, P. and Correia, a. L.: Spatial variability of the direct radiative forcing of biomass burning aerosols and the effects of
738 land use change in Amazonia, *Atmos. Chem. Phys.*, 13(3), 1261–1275, doi:10.5194/acp-13-1261-2013, 2013.
- 739 Shrivastava, M., Andreae, M. O., Artaxo, P., Barbosa, H. M. J., Berg, L. K., Brito, J., Ching, J., Easter, R. C., Fan, J., Fast, J. D., Feng, Z.,
740 Fuentes, J. D., Glasius, M., Goldstein, A. H., Alves, E. G., Gomes, H., Gu, D., Guenther, A., Jathar, S. H., Kim, S., Liu, Y., Lou, S., Martin,
741 S. T., McNeill, V. F., Medeiros, A., de Sá, S. S., Shilling, J. E., Springston, S. R., Souza, R. A. F., Thornton, J. A., Isaacman-VanWertz, G.,
742 Yee, L. D., Ynoue, R., Zaveri, R. A., Zelenyuk, A. and Zhao, C.: Urban pollution greatly enhances formation of natural aerosols over the
743 Amazon rainforest, *Nat. Commun.*, 10(1), doi:10.1038/s41467-019-08909-4, 2019.
- 744 Smith, D. M., Fiddler, M. N., Pokhrel, R. P. and Bililign, S.: Laboratory studies of fresh and aged biomass burning aerosol emitted from east
745 African biomass fuels-Part 1: Optical properties, *Atmos. Chem. Phys.*, 20(17), 10149–10168, doi:10.5194/acp-20-10149-2020, 2020.
- 746 Sun, J., Zhang, Q., Canagaratna, M. R., Zhang, Y., Ng, N. L., Sun, Y., Jayne, J. T., Zhang, X., Zhang, X. and Worsnop, D. R.: Highly time-
747 and size-resolved characterization of submicron aerosol particles in Beijing using an Aerodyne Aerosol Mass Spectrometer, *Atmos. Environ.*,
748 44(1), 131–140, doi:10.1016/j.atmosenv.2009.03.020, 2010.
- 749 Surratt, J. D., Chan, A. W. H., Eddingsaas, N. C., Chan, M., Loza, C. L., Kwan, A. J., Hersey, S. P., Flagan, R. C., Wennberg, P. O. and
750 Seinfeld, J. H.: Reactive intermediates revealed in secondary organic aerosol formation from isoprene, *Proc. Natl. Acad. Sci.*, 107(15), 6640–
751 6645, doi:10.1073/pnas.091114107, 2010.
- 752 Szopa, S., Naik, V., Artaxo, P., Berntsen, T., Collins, W. D., Fuzzi, S., Gallardo, L., Kiendler-Scharr, A., Klimont, Z., Liao, H., Unger, N.
753 and Zanis, P.: Short-lived Climate Forcers, in *Climate Change 2021 – The Physical Science Basis*, pp. 817–922, Cambridge University
754 Press., 2023.
- 755 Tuch, T. M., Haudek, A., Müller, T., Nowak, A., Wex, H. and Wiedensohler, A.: Design and performance of an automatic regenerating
756 adsorption aerosol dryer for continuous operation at monitoring sites, *Atmos. Meas. Tech.*, 2(2), 417–422, doi:10.5194/amt-2-417-2009,
757 2009.
- 758 Ulbrich, I. M., Canagaratna, M. R., Zhang, Q., Worsnop, D. R. and Jimenez, J. L.: Interpretation of organic components from Positive Matrix
759 Factorization of aerosol mass spectrometric data, *Atmos. Chem. Phys.*, 9(9), 2891–2918, doi:10.5194/acp-9-2891-2009, 2009.
- 760 Velazquez-Garcia, A., Crumeyrolle, S., de Brito, J. F., Tison, E., Bourriane, E., Chiapello, I. and Riffault, V.: Deriving composition-
761 dependent aerosol absorption, scattering and extinction mass efficiencies from multi-annual high time resolution observations in Northern
762 France, *Atmos. Environ.*, 298(December 2022), 119613, doi:10.1016/j.atmosenv.2023.119613, 2023.
- 763 Virtanen, P., Gommers, R., Oliphant, T. E., Haberland, M., Reddy, T., Cournapeau, D., Burovski, E., Peterson, P., Weckesser, W., Bright,
764 J., van der Walt, S. J., Brett, M., Wilson, J., Millman, K. J., Mayorov, N., Nelson, A. R. J., Jones, E., Kern, R., Larson, E., Carey, C. J., Polat,
765 İ., Feng, Y., Moore, E. W., VanderPlas, J., Laxalde, D., Perktold, J., Cimrman, R., Henriksen, I., Quintero, E. A., Harris, C. R., Archibald,
766 A. M., Ribeiro, A. H., Pedregosa, F., van Mulbregt, P., Vijaykumar, A., Bardelli, A. Pietro, Rothberg, A., Hilboll, A., Kloeckner, A., Scopatz,
767 A., Lee, A., Rokem, A., Woods, C. N., Fulton, C., Masson, C., Häggström, C., Fitzgerald, C., Nicholson, D. A., Hagen, D. R., Pasechnik,
768 D. V., Olivetti, E., Martin, E., Wieser, E., Silva, F., Lenders, F., Wilhelm, F., Young, G., Price, G. A., Ingold, G.-L., Allen, G. E., Lee, G.
769 R., Audren, H., Probst, I., Dietrich, J. P., Silterra, J., Webber, J. T., Slavič, J., Nothman, J., Buchner, J., Kulick, J., Schönberger, J. L., de
770 Miranda Cardoso, J. V., Reimer, J., Harrington, J., Rodríguez, J. L. C., Nunez-Iglesias, J., Kuczynski, J., Tritz, K., Thoma, M., Newville,
771 M., Kümmerer, M., Bolingbroke, M., Tartre, M., Pak, M., Smith, N. J., Nowaczyk, N., Shebanov, N., Pavlyk, O., Brodtkorb, P. A., Lee, P.,
772 McGibbon, R. T., Feldbauer, R., Lewis, S., Tygier, S., Sievert, S., Vigna, S., Peterson, S., More, S., Pudlik, T., et al.: SciPy 1.0: fundamental
773 algorithms for scientific computing in Python, *Nat. Methods*, 17(3), 261–272, doi:10.1038/s41592-019-0686-2, 2020.
- 774 Wang, Y. H., Liu, Z. R., Zhang, J. K., Hu, B., Ji, D. S., Yu, Y. C. and Wang, Y. S.: Aerosol physicochemical properties and implications for
775 visibility during an intense haze episode during winter in Beijing, *Atmos. Chem. Phys.*, 15(6), 3205–3215, doi:10.5194/acp-15-3205-2015,
776 2015.



- 777 Wennberg, P. O., Bates, K. H., Crouse, J. D., Dodson, L. G., McVay, R. C., Mertens, L. A., Nguyen, T. B., Praske, E., Schwantes, R. H.,
778 Smarte, M. D., St Clair, J. M., Teng, A. P., Zhang, X. and Seinfeld, J. H.: Gas-Phase Reactions of Isoprene and Its Major Oxidation Products,
779 *Chem. Rev.*, 118(7), 3337–3390, doi:10.1021/acs.chemrev.7b00439, 2018.
- 780 Whitehead, J. D., Darbyshire, E., Brito, J., Barbosa, H. M. J., Crawford, I., Stern, R., Gallagher, M. W., Kaye, P. H., Allan, J. D., Coe, H.,
781 Artaxo, P. and McFiggans, G.: Biogenic cloud nuclei in the central Amazon during the transition from wet to dry season, *Atmos. Chem.*
782 *Phys.*, 16(15), 9727–9743, doi:10.5194/acp-16-9727-2016, 2016.
- 783 Wiedensohler, A., Birmili, W., Nowak, A., Sonntag, A., Weinhold, K., Merkel, M., Wehner, B., Tuch, T., Pfeifer, S., Fiebig, M., Fjåraa, a.
784 M., Asmi, E., Sellegri, K., Depuy, R., Venzac, H., Villani, P., Laj, P., Aalto, P., Ogren, J. a., Swietlicki, E., Williams, P., Roldin, P., Quincey,
785 P., Hüglin, C., Fierz-Schmidhauser, R., Gysel, M., Weingartner, E., Riccobono, F., Santos, S., Gröning, C., Faloon, K., Beddows, D.,
786 Harrison, R., Monahan, C., Jennings, S. G., O’Dowd, C. D., Marinoni, A., Horn, H.-G., Keck, L., Jiang, J., Scheckman, J., McMurry, P. H.,
787 Deng, Z., Zhao, C. S., Moerman, M., Henzing, B., de Leeuw, G., Löschau, G. and Bastian, S.: Mobility particle size spectrometers:
788 harmonization of technical standards and data structure to facilitate high quality long-term observations of atmospheric particle number size
789 distributions, *Atmos. Meas. Tech.*, 5(3), 657–685, doi:10.5194/amt-5-657-2012, 2012.
- 790 Xu, L., Guo, H., Boyd, C. M., Klein, M., Bougiatioti, A., Cerully, K. M., Hite, J. R., Isaacman-VanWertz, G., Kreisberg, N. M., Knote, C.,
791 Olson, K., Koss, A., Goldstein, A. H., Hering, S. V., de Gouw, J., Baumann, K., Lee, S.-H., Nenes, A., Weber, R. J. and Ng, N. L.: Effects
792 of anthropogenic emissions on aerosol formation from isoprene and monoterpenes in the southeastern United States, *Proc. Natl. Acad. Sci.*,
793 112(1), 37–42, doi:10.1073/pnas.1417609112, 2015a.
- 794 Xu, L., Guo, H., Boyd, C. M., Klein, M., Bougiatioti, A., Cerully, K. M., Hite, J. R., Isaacman-VanWertz, G., Kreisberg, N. M., Knote, C.,
795 Olson, K., Koss, A., Goldstein, A. H., Hering, S. V., de Gouw, J., Baumann, K., Lee, S.-H., Nenes, A., Weber, R. J. and Ng, N. L.: Effects
796 of anthropogenic emissions on aerosol formation from isoprene and monoterpenes in the southeastern United States, *Proc. Natl. Acad. Sci.*,
797 112(1), 37–42, doi:10.1073/pnas.1417609112, 2015b.
- 798 Yamasoe, H. A., Artaxo, P., Miguel, A. H. and Allen, A. G.: Chemical composition of aerosol particles from direct emissions of vegetation
799 " res in the Amazon Basin : water-soluble species and trace elements, *Atmos. Environ.*, 34, 2000.
- 800 Yáñez-Serrano, A. M., Nölscher, A., C., Williams, J., Wolff, S., Alves, E., Martins, G. a., Bourtsoukidis, E., Brito, J., Jardine, K., Artaxo,
801 P. and Kesselmeier, J.: Diel and seasonal changes of biogenic volatile organic compounds within and above an Amazonian rainforest, *Atmos.*
802 *Chem. Phys.*, 15(6), 3359–3378, doi:10.5194/acp-15-3359-2015, 2015.
- 803 Yu, H., Wu, C., Wu, D. and Yu, J. Z.: Size distributions of elemental carbon and its contribution to light extinction in urban and rural
804 locations in the pearl river delta region, China, *Atmos. Chem. Phys.*, 10(11), 5107–5119, doi:10.5194/acp-10-5107-2010, 2010.
- 805 Zaveri, R. A., Wang, J., Fan, J., Zhang, Y., Shilling, J. E., Zelenyuk, A., Mei, F., Newsom, R., Pekour, M., Tomlinson, J., Comstock, J. M.,
806 Shrivastava, M., Fortner, E., Machado, L. A. T., Artaxo, P. and Martin, S. T.: Rapid growth of anthropogenic organic nanoparticles greatly
807 alters cloud life cycle in the Amazon rainforest, *Sci. Adv.*, 8(2), 1–17, doi:10.1126/sciadv.abj0329, 2022.
- 808 Zhang, Q., Jimenez, J. L., Canagaratna, M. R., Ulbrich, I. M., Ng, N. L., Worsnop, D. R. and Sun, Y.: Understanding atmospheric organic
809 aerosols via factor analysis of aerosol mass spectrometry: A review, *Anal. Bioanal. Chem.*, 401(10), 3045–3067, doi:10.1007/s00216-011-
810 5355-y, 2011.